

Data-driven Uncertainty Quantification for Systematic Coarse-grained Models

Tangxin Jin¹, Anthony Chazirakis^{2,3}, Evangelia Kalligiannaki^{2,*},
Vagelis Harmandaris^{2,3}, and Markos A. Katsoulakis²

¹ Department of Mathematics and Statistics, University of Massachusetts, Amherst, USA;

² Institute of Applied and Computational Mathematics, Foundation for Research and Technology - Hellas, Heraklion Crete, Greece;

³ Department of Mathematics and Applied Mathematics, University of Crete, Heraklion Crete, Greece;

*E-mail: evangelia.kalligiannaki@iacm.forth.gr

Abstract

In this work, we present methodologies for the quantification of confidence in bottom-up coarse-grained models for molecular and macromolecular systems. Coarse-graining methods have been extensively used in the past decades in order to extend the length and time scales accessible by simulation methodologies. The quantification, though, of induced errors due to the limited availability of fine-grained data is not yet established. Here, we employ rigorous statistical methods to deduce guarantees for the optimal coarse models obtained via approximations of the multi-body potential of mean force, with the relative entropy, the relative entropy rate minimization, and the force matching methods. Specifically, we present and apply statistical approaches, such as bootstrap and jackknife, to infer confidence sets for a limited number of samples, i.e., molecular configurations. Moreover, we estimate asymptotic confidence intervals assuming adequate sampling of the phase space. We demonstrate the need for non-asymptotic methods and quantify confidence sets through two applications. The first is a two-scale fast/slow diffusion process projected on the slow process. With this benchmark example, we establish the methodology for both independent and time-series data. Second, we apply these uncertainty quantification approaches on a polymeric bulk system. We consider an atomistic polyethylene melt as the prototype system for developing coarse-graining tools for macromolecular systems. For this system, we estimate the coarse-grained force field and present confidence levels with respect to the number of available microscopic data.

Keywords: coarse-graining; confidence; finite data; bootstrap; jackknife; asymptotic error

1 Introduction

The research in systematic bottom-up coarse-graining methods for molecular systems has significantly advanced in the past decades. When adequate information is provided through the fine-grained data, the resulting coarse force fields are describing well structural properties, [35, 49, 43, 36]. Moreover, there is active research and considerable progress on the dynamics of coarse models, [20, 21, 19, 45]. However, there is a gap in the literature regarding the quantification of the induced errors due to the limited availability of fine-grained data. In the current work, we aim to incorporate rigorous statistical methods with coarse-graining methods to provide data-driven confidence sets.

Coarse-graining (CG) is a model reduction methodology that is used in order to extend the spatio-temporal scales accessible by microscopic (atomistic) simulations and to study molecular systems properties at mesoscale regimes. Systematic (chemistry specific) CG models are obtained by lumping groups of chemically connected atoms into CG particles (or CG beads) and deriving the effective coarse-grained interaction potentials from the microscopic details of the atomistic models. Such models are capable of predicting the properties of specific systems quantitatively and have been applied with great success to a vast range of molecular systems. To build CG models, one needs to derive (a) CG interaction potentials to describe equilibrium properties and (b) dynamical models to describe kinetic properties, directly from more detailed (microscopic) simulations. The effective CG potentials approximate the many-body potential, describing the equilibrium distribution of CG particles. These CG potentials can be developed through different numerical parameterizing methods at equilibrium, such as the iterative Boltzmann inversion (IBI) [35, 49, 43], the inverse Newton (or inverse Monte Carlo) [32, 33], the force matching (FM) or Multiscale Coarse-Graining (MSCG) [24, 23], [38, 37, 39], the Relative Entropy (RE) methods [4, 48], and the cluster expansion based methods [50]. Also, during the last decade, bottom-up CG methods for treating molecular systems under non-equilibrium conditions have been developed. Such are, the recently introduced, path-space relative entropy (PSRE), relative entropy rate (RER), and path-space force matching (PSFM) methods for providing effective CG models at equilibrium, non-equilibrium, transient, or stationary time regimes, [28, 19]. The path-space methods have been further applied successfully to the dimensionality reduction of stochastic reaction networks [29], and the sensitivity analysis of molecular models [51]. All these methods fall under the umbrella of statistical inference methods. Statistical inference is our point of view in the current study from which we draw the rigorous mathematical and statistical tools, [11, 53, 52].

Quantifying parametric uncertainties accounts for assessing the model accuracy, variability, and sensitivity. Thus, naturally, a primary challenge in all above CG approaches is to quantify uncertainties in effective CG model due to the involved approximations. We are considering the (limited) size of the available microscopic data, and the numerical/algorithmic errors. Two general 'philosophies' in inferential statistics are frequentist inference and Bayesian inference. The Bayesian approach has been studied recently for the coarse-graining of molecular systems. For example, Voth and co-workers [30] have applied the empirical Bayes technique to estimate the force field parameters for the FM method. Authors in [13, 12], in addition to parameter estimation, propose a methodology for model selection based on the Bayesian approach. Furthermore, in refs. [46, 14], authors focus on the derivation of credible intervals for CG models of water. Bayesian uncertainty estimation has also been applied to parametrize atomistic molecular models in refs. [1, 2, 9, 15]. The Bayesian perspective can provide a range of probabilistic properties, but it relies on prior knowledge often not available. Thus any credible interval estimation relies on uninformative priors. In contrast, estimating frequentist parametric and non-parametric confidence intervals requires no prior information, [11].

Estimates of confidence intervals are given by asymptotic and non-asymptotic methods, chosen based on the available data. The asymptotic approach relies on the central limit theorem and the asymptotic Gaussian convergence theory. Additionally, concentration inequalities can provide reliable bound estimates for quantities of interest, [8]. The non-asymptotic methods concern estimating parameter statistics for finite data; typical examples are the jackknife and the bootstrap ones [10, 34]. Such methods have been employed in the past to obtain estimates of the parameters in classical force fields. For example, Reiher and collaborators [54, 42], employed frequentist statistical tools. Specifically, they utilize non-parametric bootstrapping, to obtain reliable estimates of the fit parameters present in semi-classical dispersion interactions based on the Density Functional Theory (DFT). Recently, authors in ref. [31] introduce a probabilistic potential ensemble method to estimate uncertainties in classical potential fitting based on DFT calculations. In addition, uncertainty quantification studies for the parameters of molecular models appear in [51] using information theory tools, and in [25] via a polynomial chaos approach.

Despite the above studies, according to our knowledge, asymptotic and non-asymptotic methods have not yet been explored in the context of CG modeling of high dimensional systems, and in particular for macromolecular systems. Here we address the accuracy of CG models for molecular systems by employing frequentist statistical data analysis. Our goal is to present and apply rigorous statistical approaches, i.e., bootstrap and jackknife, to infer confidence sets for a *limited number of samples*.

We apply these methodologies to: (a) a relatively simple benchmarking problem, of a two scale fast/slow diffusion process and (b) a realistic bulk polymer model, as a prototype example of a high dimensional macromolecular system. The latter is essential if we consider that independent data are required to deduce the confidence sets with the non-asymptotic methods, though obtaining sufficiently uncorrelated data of high molecular weight model polymers is challenging, [22, 20].

The structure of this work is as follows. Firstly, we present a short review of the bottom-up coarse-graining methodologies of molecular systems from the perspective of statistical inference. Next, we construct the asymptotic and non-asymptotic confidence intervals for the RE, RER, and FM methods. We benchmark the methodology with a multi-scale diffusion system with known corresponding stochastic averaging limits. We derive the bootstrap and jackknife estimates for the fitted interaction potential for a high dimensional polyethylene melt, based on data derived from detailed atomistic simulations. Finally, we conclude and discuss our findings.

2 Physics-based data-driven coarse-graining

Assume a prototypical problem of n particles (atoms or molecules) in a box of volume V at temperature T . Let $\mathbf{q} = (q_1, \dots, q_n) \in \mathbb{R}^{3n}$ describe the position of the particles in the atomistic (microscopic) description with potential energy $U(\mathbf{q})$. The probability of a state \mathbf{q} at the temperature T is given by the Gibbs canonical probability density

$$\mu(\mathbf{q}) = Z^{-1} \exp\{-\beta U(\mathbf{q})\}, \quad (1)$$

where $Z = \int_{\mathbb{R}^{3n}} e^{-\beta U(\mathbf{q})} d\mathbf{q}$ is the configurational the partition function, $\beta = \frac{1}{k_B T}$, and k_B is the Boltzmann constant. We should note that the studies and analyses presented in this work are performed on the configuration space. Moreover, we assume that the configurational time evolution of the particles is described by a continuous time process $\{X_t\}_{t \geq 0} = \{\mathbf{q}_t\}_{t \geq 0}$ in \mathbb{R}^{3n} , with path space distribution $P_{[0,t]}$, and Gibbs probability density (1). If we assume Markovianity, then a temporal discretization of the process leads to a Markov chain with the transition probability kernel $p(\mathbf{x}, \mathbf{x}')$.

Thus, the path space probability density of $\{X_1, \dots, X_N\}$, observed at t_1, \dots, t_N respectively, is

$$P(X_1, \dots, X_N) = \nu(X_1) \prod_{i=1}^{N-1} p(X_i, X_{i+1}), \quad (2)$$

where ν is the initial state probability density. We define coarse-graining through the configurational CG mapping $\mathbf{\Pi} : \mathbb{R}^{3n} \rightarrow \mathbb{R}^{3m}$, determining the $m (< n)$ CG particles as a function of the microscopic configuration \mathbf{q} . The mappings most commonly considered in coarse-graining of molecular systems are linearly represented by a set of non-negative real constants $\{\zeta_{ij}, i = 1, \dots, m, j = 1, \dots, n\}$, for which $\bar{\mathbf{q}}_i := \mathbf{\Pi}_i(\mathbf{q}) = \sum_j \zeta_{ij} q_j \in \mathbb{R}^3$, $i = 1, \dots, m$. The probability that the CG system has configuration $\bar{\mathbf{q}} = (\bar{q}_1, \dots, \bar{q}_m) \in \mathbb{R}^{3m}$ is $\bar{\mu}(\bar{\mathbf{q}}) = \int_{\Omega(\bar{\mathbf{q}})} \mu(\mathbf{q}) d\mathbf{q}$, $\Omega(\bar{\mathbf{q}}) = \{\mathbf{q} \in \mathbb{R}^{3n} : \mathbf{\Pi}(\mathbf{q}) = \bar{\mathbf{q}}\}$. The corresponding free energy at the CG level, described by the m -body potential of the mean force (PMF), is

$$U^{\text{pmf}}(\bar{\mathbf{q}}) = -\frac{1}{\beta} \log \int_{\Omega(\bar{\mathbf{q}})} e^{-\beta U(\mathbf{q})} d\mathbf{q}.$$

Bottom-up structural-based CG methods look for approximations of the m -body PMF $U^{\text{pmf}}(\bar{\mathbf{q}})$

$$\bar{U}(\bar{\mathbf{q}}; \theta), \quad \theta \in \Theta \subseteq \mathbb{R}^K, \quad (3)$$

which defines the corresponding approximating probability density

$$\bar{\mu}^\theta(\bar{\mathbf{q}}) = (Z^\theta)^{-1} \exp\{-\beta \bar{U}(\bar{\mathbf{q}}; \theta)\}, \quad \theta \in \Theta, \quad (4)$$

where $Z^\theta = \int_{\mathbb{R}^{3m}} e^{-\beta \bar{U}(\bar{\mathbf{q}}; \theta)} d\bar{\mathbf{q}}$ is the normalization constant.

We introduce a Markov process $\{\bar{X}_t\}_{t \geq 0}$ in \mathbb{R}^{3m} to approximate the time evolution of the coarse variables $\{\mathbf{\Pi} X_t\}_{t \geq 0}$. The CG process $\{\bar{X}_t\}_{t \geq 0}$ is defined through its parametric path space distribution

$$\bar{Q}_{[0,t]}^\theta, \quad \theta \in \Theta \subseteq \mathbb{R}^K. \quad (5)$$

The goal is to find the most effective CG model given a set of either independent and identically distributed (i.i.d.) or time-series data. In this work, we elaborate with the relative entropy minimization, relative entropy rate minimization, and the force matching methods to find the effective CG model.

I. Independent, identically distributed data. Given N i.i.d. configurational observations from the microscopic Gibbs density (1),

$$\mathcal{D}_N^{\text{iid}} = \{X_1, \dots, X_N\}, \quad (6)$$

we aim to infer the CG probability density (4).

The Force Matching method determines a CG approximating force $\bar{F}(\bar{\mathbf{q}}; \theta) = -\nabla \bar{U}(\bar{\mathbf{q}}; \theta)$, and thus an effective potential from atomistic force information, as the solution of the mean least-square minimization problem

$$\min_{\theta \in \Theta} \mathbb{E}_\mu [\|F(\mathbf{q}) - \bar{F}(\mathbf{\Pi}(\mathbf{q}); \theta)\|^2], \quad (7)$$

where $\mathbb{E}_\mu[\cdot]$ denote the average with respect to the probability density $\mu(\mathbf{q})$, and $\|\cdot\|$ the Euclidean norm in \mathbb{R}^{3m} . The reference field $F(\mathbf{q}) \in \mathbb{R}^{3m}$ is the local mean force whose component $F_I(\mathbf{q})$, $I = 1, \dots, m$ is the force exerted at the I -th CG particle and is a function of the microscopic forces. For example, if the CG particle corresponds to the center of mass of a group of atoms then $F_I(\mathbf{q}) = \sum_{j \in \{\text{group } I\}} f_j(\mathbf{q})$, $I = 1, \dots, m$, where $f_j(\mathbf{q})$ is the force exerted at the j -th microscopic

particle. Thus, given the set of i.i.d. data \mathcal{D}_N^{iid} described in (6), the discrete optimization problem corresponding to (7) is

$$\hat{\theta}_N^{iid, fm}(X_1, \dots, X_N) = \operatorname{argmin}_{\theta \in \Theta} \frac{1}{N} \sum_{i=1}^N \|F(X_i) - \bar{F}(\mathbf{\Pi}(X_i); \theta)\|^2. \quad (8)$$

The Relative Entropy minimization method determines a CG effective potential $\bar{U}(\bar{\mathbf{q}}; \theta)$ by minimizing the relative entropy $\mathcal{R}(\mu \| \mu^\theta)$ between the microscopic Gibbs measure $\mu(\mathbf{q})$ and a back-mapping $\mu^\theta(\mathbf{q}) = \bar{\mu}^\theta(\bar{\mathbf{q}})\nu(\mathbf{q}|\bar{\mathbf{q}})$ of the approximate CG measure $\bar{\mu}^\theta(\bar{\mathbf{q}})$. That is

$$\min_{\theta \in \Theta} \mathcal{R}(\mu \| \mu^\theta), \quad (9)$$

where

$$\mathcal{R}(\mu \| \mu^\theta) = \mathbb{E}_\mu \left[\log \frac{\mu(\mathbf{q})}{\mu^\theta(\mathbf{q})} \right].$$

Thus, the RE estimator for the CG model is

$$\hat{\theta}_N^{iid, re}(X_1, \dots, X_N) = \operatorname{argmin}_{\theta \in \Theta} \frac{1}{N} \sum_{i=1}^N \log \frac{\mu(X_i)}{\bar{\mu}^\theta(\mathbf{\Pi}X_i)}, \quad (10)$$

assuming that the back-mapping distribution does not depend on θ .

II. Time-series data. In path space we estimate the probability density (5) at dynamical regimes, given N_p i.i.d. path observations

$$\mathcal{D}_{N_p, N_t}^{ts} = \{X_1^k, \dots, X_{N_t}^k\}_{k=1}^{N_p}, \quad (11)$$

from the microscopic path space probability density (2). Each path (or trajectory) observation consists of N_t discrete time observations, which, for simplicity, we consider of uniform time step. Also, each path observation can have different size N_k , $k = 1, \dots, N_p$.

The best approximation is given by entropy based criteria to find the best Markovian approximation of the coarse-grained process. The optimization principle is defined in terms of the path-space relative entropy,

$$\min_{\theta \in \Theta} \mathcal{R}(P_{[0,t]} \| Q_{[0,t]}^\theta), \quad (12)$$

where $Q_{[0,t]}^\theta := \mathbf{\Pi}_*^\dagger \bar{Q}_{[0,t]}^\theta$ is the back-mapping to the microscopic space of the parameterized path-space coarse-grained distribution. The relative entropy rate (RER) is defined by

$$\mathcal{H}(P | Q^\theta) := \lim_{t \rightarrow \infty} \frac{1}{t} \mathcal{R}(P_{[0,t]} \| Q_{[0,t]}^\theta).$$

Therefore, the minimization of the RER

$$\min_{\theta \in \Theta} \mathcal{H}(P | Q^\theta),$$

is the appropriate optimization problem for $t \rightarrow \infty$, and for stationary Markov processes [28]. In work [19], we prove that the path-space variational inference problem (12) in continuous time reduces to a path-space force matching optimization, for a class of CG mappings. In addition, the RER reduces to the FM for stationary processes with invariant probability density $\mu(\mathbf{q})$ defined in (1).

For discrete time observations the CG path-space distribution (5), assuming Markovianity for the CG model, is

$$\bar{Q}^\theta(\bar{X}_1, \dots, \bar{X}_N) = \bar{\nu}(\bar{X}_1) \prod_{i=1}^{N-1} \bar{q}^\theta(\bar{X}_i, \bar{X}_{i+1}),$$

where $\bar{q}^\theta(\bar{\mathbf{x}}, \bar{\mathbf{x}}')$ is the transition probability kernel of the proposed approximate CG process, and $\bar{\nu}(\bar{\mathbf{x}})$ denotes the initial distribution. Introducing an unbiased estimator for the relative entropy, the optimal parameter estimate for $\mathcal{D}_{N_p, N_t}^{ts}$ is given by

$$\hat{\theta}_{N_p, N_t}^{ts}(X_1^1, \dots, X_{N_t}^{N_p}) = \underset{\theta \in \Theta}{\operatorname{argmin}} \frac{1}{N_p} \sum_{k=1}^{N_p} \log \frac{P(X_1^k, X_2^k, \dots, X_{N_t}^k)}{\bar{Q}^\theta(\mathbf{\Pi}X_1^k, \mathbf{\Pi}X_2^k, \dots, \mathbf{\Pi}X_{N_t}^k)}, \quad (13)$$

where we assume that the $Q_{[0,t]}^\theta$ in relation (12) is given as the product of \bar{Q}^θ and a back-mapping probability independent of θ , which for notation simplicity we do not present here. In terms of the transition probability kernels, the parameter estimator is

$$\hat{\theta}_{N_p, N_t}^{ts}(X_1^1, \dots, X_{N_t}^{N_p}) = \underset{\theta \in \Theta}{\operatorname{argmin}} \frac{1}{N_p} \sum_{k=1}^{N_p} \frac{1}{N_t - 1} \sum_{i=1}^{N_t-1} \log \frac{p(X_i^k, X_{i+1}^k)}{\bar{q}^\theta(\mathbf{\Pi}X_i^k, \mathbf{\Pi}X_{i+1}^k)}. \quad (14)$$

Note that when the time series are stationary, then they are statistically indistinguishable and the path-space optimization problem (14) reduces to the RER optimization, [19]. That is, for observations $\mathcal{D}_{N_t} = \{X_1, \dots, X_{N_t}\}$ the optimal parameter set is given by

$$\hat{\theta}_{N_t}^{ts}(X_1, \dots, X_{N_t}) = \underset{\theta \in \Theta}{\operatorname{argmin}} \frac{1}{N_t - 1} \sum_{i=1}^{N_t-1} \log \frac{p(X_i, X_{i+1})}{\bar{q}^\theta(\mathbf{\Pi}X_i, \mathbf{\Pi}X_{i+1})}. \quad (15)$$

The RER estimator becomes the RE estimator when the samples are replaced by i.i.d. generated from the stationary probability distribution $\mu(\bar{\mathbf{q}})$ and $\bar{q}^\theta(\mathbf{\Pi}X_i, \mathbf{\Pi}X_{i+1}) = \bar{\mu}(\mathbf{\Pi}X_{i+1}; \theta)$.

Note, that the major difference between the RE minimization and the RER minimization is that in the first we need i.i.d. data from $\mu(\bar{\mathbf{q}})$ while in later we need time series data from $P_{[0,t]}$. This is an advantage of the path-space methods since there is no computational effort to generate the i.i.d. data. On the other hand, due to the ergodic theory, when the time-series data is long enough we can substitute the configuration space average with the time space average where correlated data are admissible. Thus, the effort to generate i.i.d. data is transferred to the effort to generate long time correlated data.

3 Confidence intervals for coarse-grained methods

In this section, we assess the uncertainty of the estimated parameters θ , as well as quantities of interest given as composite functions of the parameters. Specifically, we construct confidence intervals (CIs) on the CG model parameters for a given set of data for both equilibrium and path-space models. We demonstrate the methodology of constructing non-asymptotic and asymptotic confidence intervals in detail for the relative entropy estimation $\hat{\theta}_N^{iid, re}$. The methodology is also valid for the force matching estimation $\hat{\theta}_N^{iid, fm}$, if we consider it as a regression problem with the corresponding likelihood, which is proportional to $\exp\{-\|F(\bar{\mathbf{q}}) - \bar{F}(\bar{\mathbf{q}}; \theta)\|^2\}$.

3.1 Statistical estimation and path-space relative entropy optimization

As described in the previous section, we consider two types of data; i.e., sets of configurations derived from the more detailed microscopic simulations in the form of: (a) *independent and identically distributed* data, \mathcal{D}_N^{iid} generated from the invariant distribution μ , and (b) *discrete time-series* data $\mathcal{D}_{N_p, N_t}^{ts}$, eq. (11), generated from the path distribution of the original microscopic process $P_{[0,t]}$. Note that eq. (10) simplifies further since the invariant measure μ is independent of θ ,

$$\hat{\theta}_N^{iid, re}(X_1, \dots, X_N) = \operatorname{argmax}_{\theta \in \Theta} \frac{1}{N} \sum_{i=1}^N \log \bar{\mu}^\theta(\mathbf{\Pi} X_i). \quad (16)$$

For the time-series data the optimization problem (15) is equivalent to

$$\hat{\theta}_{N_p N_t}^{ts}(X_1^1, \dots, X_{N_t}^{N_p}) = \operatorname{argmax}_{\theta \in \Theta} \frac{1}{N_p} \sum_{k=1}^{N_p} \frac{1}{N_t - 1} \sum_{i=1}^{N_t-1} \log \bar{q}^\theta(\mathbf{\Pi} X_i^k, \mathbf{\Pi} X_{i+1}^k). \quad (17)$$

Thus, to derive the optimal CG model parameter, in both cases, we need (a) the data from the microscopic process, (b) the pre-defined CG mapping $\mathbf{\Pi}$, and (c) the parameterized coarse-grained model. These characterize the data and physics driven nature of the coarse-graining approach, which relates the true CG model to its digital-twin, the approximate CG model, [18].

However, in many situations only a small number N of data is available due to the extreme cost to generate them, either experimentally or numerically. This is precisely the case in the coarse-graining of macromolecular (polymeric) systems, where the cost to generate i.i.d. samples increases strongly with the molecular length. For example, for polymer melts, the maximum relaxation time of entangled linear chains scales with the cubic power of their length; for other architectures the dependence is even stronger, e.g., for star polymers becomes exponential [7]. This is evident in section 5, where we derive the optimal CG force field for a polyethylene melt and the corresponding confidence intervals.

3.2 Non-asymptotic confidence intervals

There is a vast need for statistical information about parameters in CG models, especially when the size of data is limited. Such information would provide estimates of whether those parameters are in a reasonable region, and whether they are sensitive to the data. Here we present two statistically rigorous non-asymptotic methods to compute standard errors and construct confidence intervals, namely the jackknife and the bootstrap [53, 11]. These techniques are valid for the i.i.d. case \mathcal{D}_N^{iid} , as well as for multiple i.i.d. time-series $\mathcal{D}_{N_p N_t}^{ts}$, but not for the correlated data of a single time-series. We will apply the jackknife and bootstrap methods to construct confidence bounds for the CG parameters.

3.2.1 The Jackknife

Let us denote $\hat{\theta}_N = \hat{\theta}_N^{iid}$ and $\hat{\theta}_{(-i)}$ the estimators of the CG parameters, from $\mathcal{D}_N = \{X_1, \dots, X_N\}$ and with the i -th observation X_i removed respectively, i.e.,

$$\hat{\theta}_{(-i)} = \hat{\theta}_{N-1}(X_1, \dots, X_{i-1}, X_{i+1}, \dots, X_n).$$

Let also \tilde{T}_i be the pseudo-values

$$\tilde{T}_i = N\hat{\theta}_N - (N-1)\hat{\theta}_{(-i)}.$$

Then, the jackknife variance estimation is

$$V_{jack} = \frac{\sum_{i=1}^N \left(\tilde{T}_i - \frac{1}{n} \sum_{i=1}^N \tilde{T}_i \right)^2}{N(N-1)} = \frac{N-1}{N} \sum_{i=1}^N \left(\hat{\theta}_{(-i)} - \frac{1}{N} \sum_{i=1}^N \hat{\theta}_{(-i)} \right)^2,$$

and the corresponding standard confidence interval is

$$CI_{jack} = \left[\hat{\theta}_N - z_{\alpha/2} \sqrt{V_{jack}}, \quad \hat{\theta}_N + z_{\alpha/2} \sqrt{V_{jack}} \right]. \quad (18)$$

The jackknife method consistently estimates the variance of $\hat{\theta}_N$, though it cannot produce consistent estimates of the standard error of sample quantiles. The bootstrap method, on the other hand, is able to produce not only variance estimation but also quantile estimates and thus non-symmetric confidence intervals, as discussed below.

3.2.2 The Bootstrap

To construct bootstrap confidence intervals, firstly we assume that the empirical distribution of the data \mathcal{D}_N is \hat{F}_N mimicking the true distribution. Then, B bootstrap samples are generated i.e., B sets of samples X_1^*, \dots, X_N^* are drawn from \hat{F}_N . The procedure is described by the following steps:

1. Draw N new samples $X_1^*, \dots, X_N^* \sim \hat{F}_N$, i.e., draw X_i^* randomly from $\mathcal{D}_N = \{X_1, \dots, X_N\}$ with equal probability and with replacement.
2. Compute $\hat{\theta}^*$ according to the chosen estimator, e.g., (16) for i.i.d data.
3. Repeat steps 1 and 2, B times to get $\hat{\theta}_1^*, \dots, \hat{\theta}_B^*$.

With this procedure we construct an approximate distribution of the statistical estimator $\hat{\theta}_N$. There are several approaches to construct bootstrap confidence intervals, such as the standard, the pivotal, the percentile, and the bootstrap-t intervals, [11], [53]. In the current work, we estimate the standard and percentile confidence intervals which we present next. The bootstrap variance estimation is

$$V_{boot} = \frac{1}{B} \sum_{i=1}^B \left(\hat{\theta}_i^* - \frac{1}{B} \sum_{b=1}^B \hat{\theta}_b^* \right)^2, \quad (19)$$

and the bootstrap standard confidence interval is

$$CI_{s,boot} = \left[\hat{\theta}_N - z_{\alpha/2} \sqrt{V_{boot}}, \quad \hat{\theta}_N + z_{\alpha/2} \sqrt{V_{boot}} \right]. \quad (20)$$

The bootstrap percentile confidence interval is given directly from the bootstrap distribution of the statistical estimator $\hat{\theta}$, and is

$$CI_{p,boot} = \left[\hat{\theta}_{\alpha/2}^*, \quad \hat{\theta}_{1-\alpha/2}^* \right], \quad (21)$$

where $\hat{\theta}_{\alpha/2}^*$ is the $\alpha/2$ percentile of $\hat{\theta}_1^*, \dots, \hat{\theta}_B^*$.

The percentile bootstrap intervals are not accurate though if bootstrap estimates are highly biased and skewed. Highly biased bootstrap estimates can not represent the true distribution, and highly skewed bootstrap estimates concentrate more on one side of the distribution and thus has a

long tail on the other side. There are improved intervals but more complicated, such as the bias-corrected and accelerated bootstrap (BCa). BCa corrects for bias and skewness in the distribution of bootstrap estimates and improves the coverage accuracy of standard intervals from first order to second order, thus provides reasonably narrow intervals but is complicated to implement [6]. Both techniques, the jackknife, and bootstrap use part of the data to get several estimators for the parameters and then use those estimators to construct confidence intervals. Bootstrap can have higher computational cost if the number of bootstrap samples (B) is larger than the number of data (N), which is often the case. Thus, the jackknife method is less computationally expensive but is less general. As reported in literature, [11], empirical evidence suggests that $B = 200$ is usually sufficient for evaluating the bootstrap estimate of the standard error, but larger values should be considered for the bootstrap confidence intervals.

3.3 Asymptotic confidence intervals

I. Independent, identically distributed data. Recall that for i.i.d. data, the RE optimal parameter is

$$\hat{\theta}_N^{iid} = \operatorname{argmax}_{\theta \in \Theta} \frac{1}{N} \sum_{i=1}^N \log \bar{\mu}^\theta(\mathbf{I}X_i).$$

Note that $\hat{\theta}_N^{iid}$ is similar to the maximum likelihood estimator, [11]. The difference is that the maximum likelihood estimator assumes that $\mathbf{I}X_i$ has measure $\bar{\mu}^\theta$, while this assumption is not true here. Thus, a confidence interval directly obtained from maximum likelihood estimator is inaccurate. We resolve this issue by constructing a slightly different confidence interval along with two versions of the Fisher information:

$$\begin{aligned} \hat{\mathcal{F}}_1 &= -\frac{1}{N} \sum_{i=1}^N \nabla_\theta^2 \log \bar{\mu}^\theta(\mathbf{I}X_i)|_{\theta=\hat{\theta}_N^{iid}}, \\ \hat{\mathcal{F}}_2 &= \frac{1}{N} \sum_{i=1}^N (\nabla_\theta \log \bar{\mu}^\theta(\mathbf{I}X_i))(\nabla_\theta \log \bar{\mu}^\theta(\mathbf{I}X_i))^T|_{\theta=\hat{\theta}_N^{iid}}. \end{aligned}$$

These two Fisher information matrices are close if $\mathbf{I}X_i$ has distribution $\bar{\mu}^\theta$ and under the assumption that N is large enough (see Corollary 1.1.3 in supplementary information). Whether $\hat{\mathcal{F}}_1$ is close to $\hat{\mathcal{F}}_2$ could be an indirect indicator of whether the parameterized CG distribution $\bar{\mu}^\theta$ can mimic the distribution of $\mathbf{I}X_i$. That is, $\hat{\mathcal{F}}_1$ is close to $\hat{\mathcal{F}}_2$ indicates that $\mathbf{I}X_i$ has a measure close to $\mu^{\theta^{iid}}$, which means that the parameterized family of μ^θ can reconstruct the distribution of $\mathbf{I}X_i$. But the inverse might not be true in general. The asymptotic theory provides the $1 - \alpha$ confidence interval for θ in the equilibrium model (see Theorem 1.1.1 in supplementary information), which is

$$CI_{iid} = \left[\hat{\theta}_N^{iid} - \frac{z_{\alpha/2}}{\sqrt{N}} \sqrt{\hat{\mathcal{F}}_1^{-T} \hat{\mathcal{F}}_2 \hat{\mathcal{F}}_1^{-1}}, \quad \hat{\theta}_N^{iid} + \frac{z_{\alpha/2}}{\sqrt{N}} \sqrt{\hat{\mathcal{F}}_1^{-T} \hat{\mathcal{F}}_2 \hat{\mathcal{F}}_1^{-1}} \right]. \quad (22)$$

II. Time-series data. In the path-space models, the result is similar to the one in the equilibrium models where $\bar{\mu}^\theta$ is replaced by transition probability density \bar{q}^θ and a more complicated Fisher information. Recall that

$$\hat{\theta}_N^{ts} = \operatorname{argmax}_{\theta \in \Theta} \frac{1}{N-1} \sum_{i=1}^{N-1} \log \bar{q}^\theta(\mathbf{I}X_i, \mathbf{I}X_{i+1}).$$

The first Fisher information matrix

$$\hat{I}_1 = -\frac{1}{N-1} \sum_{i=1}^{N-1} \nabla_{\theta}^2 \log \bar{q}^{\theta}(\mathbf{X}_i, \mathbf{X}_{i+1})|_{\theta=\hat{\theta}_N^{ts}},$$

while the second Fisher information matrix is given by the Markov chain central limit theorem and is estimated by a batch means estimator, [26, 27]

$$\hat{I}_{2,BM} = \frac{b}{a-1} \sum_{j=1}^a (\bar{Y}_j - \bar{Y}),$$

where $\bar{Y}_j = \frac{1}{b} \sum_{i=(j-1)b+1}^{jb} \log \bar{q}^{\hat{\theta}_N^{ts}}(\mathbf{X}_i, \mathbf{X}_{i+1})$, $\bar{Y} = \frac{1}{N-1} \sum_{i=1}^{N-1} \log \bar{q}^{\hat{\theta}_N^{ts}}(\mathbf{X}_i, \mathbf{X}_{i+1})$ and $N = ab$. Thus the $1 - \alpha$ confidence interval for θ in the path-space models is

$$CI_{ts} = \left[\hat{\theta}_N^{ts} - \frac{z_{\alpha/2}}{\sqrt{N-1}} \sqrt{\hat{I}_1^{-T} \hat{I}_{2,BM} \hat{I}_1^{-1}}, \quad \hat{\theta}_N^{ts} + \frac{z_{\alpha/2}}{\sqrt{N-1}} \sqrt{\hat{I}_1^{-T} \hat{I}_{2,BM} \hat{I}_1^{-1}} \right]. \quad (23)$$

In the supplementary information accompanying this work, we present the mathematical justification for the confidence intervals provided here.

3.4 Estimating quantities of interest

Thus far, we have estimated the coarse model parameters and assessed their accuracy. Now, our interest is in finding an estimator and their uncertainty for quantities of interest (QoI),

$$\tau = g(\theta), \quad (24)$$

which are functions of θ . Given a data set \mathcal{D}_N^{iid} , the invariance principle ensures that the MLE estimator of the QoI τ , is

$$\hat{\tau} = \hat{\tau}(X_1, \dots, X_N) = g\left(\hat{\theta}_N(X_1, \dots, X_N)\right), \quad (25)$$

where $\hat{\theta}_N$ is the set of estimated model parameters, [3, 53].

The delta method provides asymptotic standard errors for $\hat{\tau}$

$$\hat{s}e(\hat{\tau}) = \sqrt{(\hat{\nabla}g)^{tr} \hat{J}_N \hat{\nabla}g},$$

where $\hat{J}_N = \hat{\mathcal{F}}_1^{-1}$, and $\hat{\nabla}g$ is $\nabla g = \left(\frac{\partial g}{\partial \theta_1}, \dots, \frac{\partial g}{\partial \theta_K}\right)^{tr}$ evaluated at $\theta = (\hat{\theta}_N)$. Here $(\cdot)^{tr}$ denotes matrix transpose.

The non-parametric resampling methods, jackknife and bootstrap described in 3.2, apply straightforwardly on $\hat{\tau}(X_1, \dots, X_N)$ through θ_N and the use of the invariance property. Indeed, the percentile bootstrap CI is

$$CI_{p,boot}^{qoi} = \left[\hat{\tau}_{\alpha/2}^*, \quad \hat{\tau}_{1-\alpha/2}^* \right], \quad (26)$$

where $\hat{\tau}_{\alpha/2}^*$ is the $\alpha/2$ percentile of $\hat{\tau}_1^*, \dots, \hat{\tau}_B^*$, and $\hat{\tau}^* = \hat{\tau}(X_1^*, \dots, X_N^*)$, for a bootstrap sample (X_1^*, \dots, X_N^*) , described in section 3.2.2.

Remark. Bayesian analysis can provide a range of information about the model through the posterior probability distribution of the model parameters. Credible intervals are thus obtained from the posterior. However, the need for prior information for the parameters is a drawback, since it is often not available. Of course, there exist techniques to overcome this, such as uninformative priors and hyper-parameters, but still some prior knowledge is necessary. In contrast, frequentist parametric and non-parametric confidence intervals require no prior information. Also, the non-parametric, uninformative posterior distribution can be approximately represented by a bootstrap distribution which may be much easier to obtain, [17].

4 Test-bed 1: Two-scale diffusion processes

In this section, we benchmark our methodology by considering a two-dimensional two-scale diffusion process. This diffusion process is a good, relatively simple, example that allows us to (a) test and compare the accuracy of the estimated parameters by the different optimization methods, (b) provide the corresponding confidence intervals, and (c) validate the results since we know the effective dynamics analytically.

The two-scale diffusion process consists of a slow variable $X_t^\epsilon \in \mathbb{R}$ and a fast variable $Y_t^\epsilon \in \mathbb{R}$, for $t \geq 0$, which satisfy the system of stochastic differential equations,

$$\begin{aligned} dX_t^\epsilon &= -Y_t^\epsilon dt + dW_t^1, \\ dY_t^\epsilon &= -\epsilon^{-1}(Y_t^\epsilon - X_t^\epsilon)dt + \epsilon^{-0.5}dW_t^2, \end{aligned} \quad (27)$$

for $\epsilon > 0$, where dW_t^1 and dW_t^2 are independent standard Wiener processes, [40]. As $\epsilon \rightarrow 0$, X_t^ϵ follows the effective process \hat{X}_t which is proved to satisfy, by the averaging principle, [16]

$$d\hat{X}_t = -\hat{X}_t dt + d\hat{W}_t. \quad (28)$$

Note that the effective potential driving the process \hat{X}_t is the harmonic potential $U(x) = \frac{1}{2}x^2$, depicted in Figure 1.

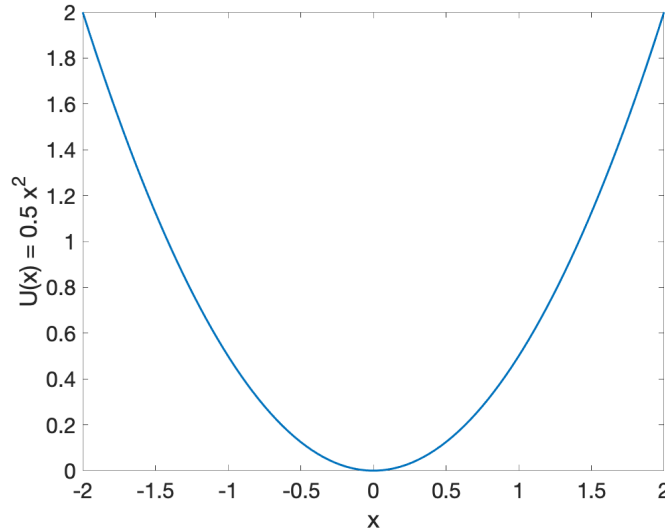


Figure 1: The effective potential for the coarse process \hat{X}_t is the harmonic interaction potential.

We are interested in constructing a coarse-grained model for the slow variable X_t^ϵ and for a finite value of $\epsilon > 0$. Thus, the CG map is $\Pi : (X_t^\epsilon, Y_t^\epsilon) \rightarrow X_t^\epsilon$. The CG process X_t^{CG} , approximating $\Pi(X_t^\epsilon, Y_t^\epsilon)$, is assumed to satisfy

$$dX_t^{CG} = a(X_t^{CG}; \theta)dt + dW_t, \quad (29)$$

where W_t is a standard Wiener process. To approximate the coarse-grained dynamics we propose an effective drift

$$a(x; \theta) = \sum_{k=1}^K \theta_k x^{k-1}, \quad (30)$$

that is an approximation over the set of polynomials $\{1, x, \dots, x^{K-1}\}$. In the example presented we choose $K = 5$. Note that in this example, we expect that the estimated parameters of the coarse grained model are close to $\theta^* = [0, -1, 0, 0, 0]$, due to the known analytical form of the effective dynamics for the process, (28). We present next a comparison between (28) and (29) by investigating the uncertainty of parameters through confidence intervals.

I. Independent, identically distributed data. Firstly, we investigate the results with i.i.d data $\mathcal{D}_N = \{(X_i, Y_i)\}_{i=1}^N$, corresponding to the invariant density of (27). We omit the notation of ϵ -dependence for notation simplicity. We minimize the RE between the invariant densities of X_t^ϵ and of X_t^{CG} . The invariant density of X_t^{CG} is

$$\bar{\mu}^\theta(x) = \frac{1}{Z^\theta} e^{-2\bar{U}(x;\theta)},$$

where $\bar{U}(x;\theta)$ is defined by $a(x;\theta) = -\frac{d}{dx}\bar{U}(x;\theta)$ and $Z^\theta = \int e^{-2\bar{U}(x;\theta)} dx$. The optimal parameter is given by

$$\begin{aligned} \theta^{iid, re} &= \operatorname{argmax}_{\theta \in \Theta} \mathbb{E}_\mu[\log \bar{\mu}^\theta \circ \mathbf{\Pi}] \\ &= \operatorname{argmax}_{\theta \in \Theta} \left\{ -2\mathbb{E}_\mu[\bar{U}(\cdot; \theta)] - \log Z^\theta \right\}. \end{aligned} \quad (31)$$

The RE estimator is described in eq. (16), while the optimization method in section 2.3 of the supplementary information. We also apply the FM method for which the optimal parameter estimator is

$$\hat{\theta}_N^{iid, fm} = \operatorname{argmin}_{\theta \in \Theta} \frac{1}{N} \sum_{i=1}^N |Y_i + a(X_i; \theta)|^2. \quad (32)$$

II. Time-series data. Secondly, we estimate the parameter for time-series data $\mathcal{D}_{N_p, N_t} = \{(X_i^k, Y_i^k)\}_{k=1, i=1}^{N_p, N_t}$. The approximate transition probability density of (29) is

$$q_h^\theta(X_i, X_{i+1}) = \frac{1}{z} e^{-\frac{1}{2h^2}|X_{i+1} - X_i - a(X_i; \theta)h|^2}, \quad (33)$$

where z is a normalized factor independent of θ , h is the discretization time step for the Euler-Maruyama approximation of X_t^{CG} with corresponding transition density $q_h^\theta(x, x')$. For multiple time-series data \mathcal{D}_{N_p, N_t} , the appropriate estimator is the path-space RE (PSRE). The optimal estimate given by the minimization problem (17) is

$$\hat{\theta}_N^{ts, psre} = \operatorname{argmin}_{\theta \in \Theta} \frac{1}{N_p} \sum_{k=1}^{N_p} \frac{1}{N_t - 1} \sum_{i=1}^{N_t - 1} |X_{i+1}^k - X_i^k - a(X_i^k; \theta)h|^2. \quad (34)$$

The corresponding RER estimator, valid for a long, stationary time series, is

$$\hat{\theta}_N^{ts, rer} = \operatorname{argmin}_{\theta \in \Theta} \frac{1}{N_t - 1} \sum_{i=1}^{N_t - 1} |X_{i+1} - X_i - a(X_i; \theta)h|^2. \quad (35)$$

as described in section 2. Moreover, in the equilibrium region the RER minimization is equivalent to the FM minimization. We describe the proof in section 2.2 of the supplementary information.

III. Asymptotic results. We begin with reporting the results for a ‘large’ sample size and the corresponding asymptotic confidence intervals as described in section 3. In all the numerical tests we fix $\epsilon = 0.005$ and $h = 0.01$. For the RE estimation, (31), we applied the Newton-Raphson (NR) algorithm. To estimate the normalization parameter Z^θ which changes at each NR iteration, we generated 5,000 CG i.i.d. samples from $\bar{\mu}^\theta(x)$ with a Hamiltonian Monte Carlo sampler. The NR algorithm converged after 20 iterations, with initial value of θ near θ^* . The details of the NR method are described in the supplementary information. For the FM and RER estimation we solve the corresponding least squares problem described in (32) and (35).

Firstly, we generate two sets of samples: (a) \mathcal{D}_N , i.i.d. samples from the invariant distribution of the exact process with $N = 500$, and (b) \mathcal{D}_{N_t} one time-series samples with $N_t = 50,000$. Note that we have experimented with various values of N and N_t . We chose to report the $N = 500$ and $N_t = 50,000$ so that the optimization methods show variance estimates of the same order.

Figures 2 and 3 show the results for the FM and the relative entropy minimization with $N = 500$ i.i.d. data respectively. In both figures, the right hand side depicts the invariant probability density function of the estimated coarse process X_t^{CG} and of the exact process X_t^ϵ . The left hand side figure presents the estimated parameters and the corresponding 95% asymptotic standard confidence interval, defined in (22). Similarly, figure 4 depicts the parameter estimates with the asymptotic CI and the invariant probability density functions of the estimated and the exact process with one correlated time-series with time step $h = 0.01$ and size $N_t = 50,000$. Also, in table 1 we present the point parameter estimates, the asymptotic variance and the computational cost for the RE, the FM and the RER optimization methods.

Method	$\hat{\theta}$	$\hat{\sigma}^2$	CI	Number of samples	CPU time (sec)
FM	$\begin{bmatrix} 0.0236 \\ -1.0240 \\ 0.0039 \\ -0.0012 \\ -0.0338 \end{bmatrix}$	$\begin{bmatrix} 0.0021 \\ 0.0063 \\ 0.0138 \\ 0.0023 \\ 0.0019 \end{bmatrix}$	$\begin{bmatrix} -0.0663 & 0.1135 \\ -1.1790 & -0.8689 \\ -0.2265 & 0.2342 \\ -0.0947 & 0.0922 \\ -0.1189 & 0.0513 \end{bmatrix}$	500	0.02
RE	$\begin{bmatrix} 0.0247 \\ -0.9827 \\ 0.0260 \\ -0.0640 \\ 0.0001 \end{bmatrix}$	$\begin{bmatrix} 0.0046 \\ 0.0261 \\ 0.0439 \\ 0.0145 \\ 0.0048 \end{bmatrix}$	$\begin{bmatrix} -0.1390 & 0.1151 \\ -1.2287 & -0.7505 \\ -0.3005 & 0.3572 \\ -0.1345 & 0.1509 \\ -0.0913 & 0.0572 \end{bmatrix}$	500	5.32
RER	$\begin{bmatrix} 0.0746 \\ -0.9805 \\ 0.0483 \\ -0.0313 \\ -0.0255 \end{bmatrix}$	$\begin{bmatrix} 0.0040 \\ 0.0112 \\ 0.0158 \\ 0.0040 \\ 0.0013 \end{bmatrix}$	$\begin{bmatrix} -0.0491 & 0.1983 \\ -1.1876 & -0.7733 \\ -0.1979 & 0.2944 \\ -0.1550 & 0.0925 \\ -0.0965 & 0.0455 \end{bmatrix}$	50,000	0.19

Table 1: Parameter and asymptotic variance estimates for ‘large sample’ sets for the two-scale diffusion benchmarking problem. The exact parameters for $\epsilon \rightarrow 0$ are $\theta^* = [0, -1, 0, 0, 0]$.

All methods approximate well the expected $\theta^* = [0, -1, 0, 0, 0]$, corresponding to the asymptotic model as $\epsilon \rightarrow 0$, as θ^* falls into the confidence interval for all methods. The RE method presents larger asymptotic variance compared to the FM. Moreover, the RE has higher computational cost than the FM. Its benefit though is the better estimation of the ‘true’ probability density, which in return will give better estimations of quantities of interest given as expected values. We can notice an excellent match of the CG invariant density with RE estimation to the exact one, while there is

a small difference with the FM and RER estimation. We attribute this difference to the fact the RE matches directly the probability densities while the FM and RER match the drift terms (i.e. the force).

Next, we comment on the FM and the RER methods from the point of view of comparing an i.i.d. method and a path-space method. The results show that we can achieve estimates with the same order of magnitude with the FM with i.i.d. data and the RER with correlated data if we use about hundred times more data in the later. This naturally increases the computational cost of the optimization problem. However, there is a computational benefit on the generation of the samples, since for the path-space samples (time series) we do not need to reject any generated data. On the contrary, to generate the i.i.d. observations we have to reject a large number of simulated data. This is extremely insufficient in high dimensional applications, as in long polymer chains discussed in the next section. Therefore the path-space methods can be advantageous when we have to generate high-dimensional samples.

On the other hand, the ergodic theory ensures that we can apply the FM method for correlated time series data, as long as the time-series is long enough. Therefore, our next numerical study examines the validity of the FM for short and long correlated time-series. That is, we use the FM estimator for correlated data, and thus introduce the estimator for time series data $\mathcal{D}_{N_p N_t}$

$$\hat{\theta}_N^{ts, fm} = \operatorname{argmin}_{\theta \in \Theta} \frac{1}{N_p} \sum_{k=1}^{N_p} \frac{1}{N_t} \sum_{i=1}^{N_t} |Y_i^k + a(X_i^k; \theta)|^2. \quad (36)$$

Table 2 reports the point estimates for time correlated samples, resulting from the FM estimator (36) and the PSRE (and RER) estimator (35). The table with the estimates for all parameters is provided the supplementary information. We observe that the FM point estimates improve as the size of the time-series increases, as expected. Comparing the $N_t = 50,000$ for the FM and the $N_p = 100, N_t = 500$ cases for which the number of samples is the same, they both yield estimates close to the truth. We notice that the FM estimator gives slightly better estimates than the PSRE estimator for short time trajectories, e.g., $N_t = 500, N_t = 5,000$. We ascribe this difference to that the first uses all fine-scale observations (X_i, Y_i) , while the latter only uses the partial observations (X_i) . To have thus reliable PSRE estimates, we need to guarantee either the trajectory is long enough or the number of trajectories is large enough. Important to note is that for the RER, we can estimate the asymptotic CIs while the FM CIs are no longer valid.

N_p	N_t	$\hat{\theta}_N^{ts, fm}$	$\hat{\theta}_N^{ts, psre}$
1	500	-0.4328	-6.0944
1	5,000	-0.9485	-1.1251
1	50,000	-0.9734	-0.9805
10	500	-0.8960	-1.3288
100	500	-0.9728	-0.7976
100	5,000	-0.9777	-0.9673

Table 2: Point estimates for the $\theta_2 = -1$, with correlated time-series data, and with the different estimators (36) and (34) for the FM and PSRE. Note that the point estimates by FM (36) has the same form with FM estimator.

IV. Non-asymptotic results. For a 'small' number of samples we test the case (a) of i.i.d. samples with $N = 50, 100, 200$, and 500 and (b) of multiple i.i.d. trajectories consisting of correlated

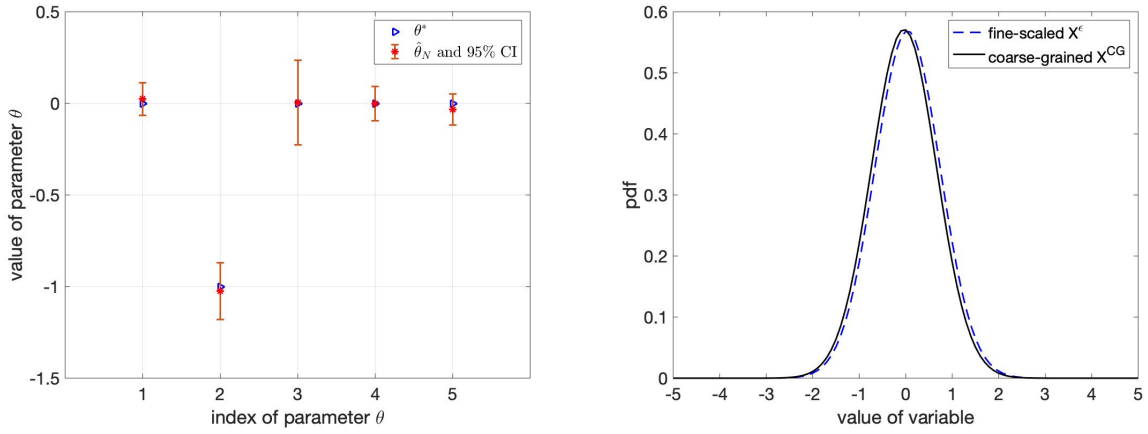


Figure 2: The estimator and 95% confidence intervals for FM method is shown on the left. The expected values $[0,-1,0,0,0]$ are located inside the intervals. A distribution of constructed CG variable by using $\hat{\theta}_N$ and a comparison with fine-scaled X^ϵ is shown on the right.

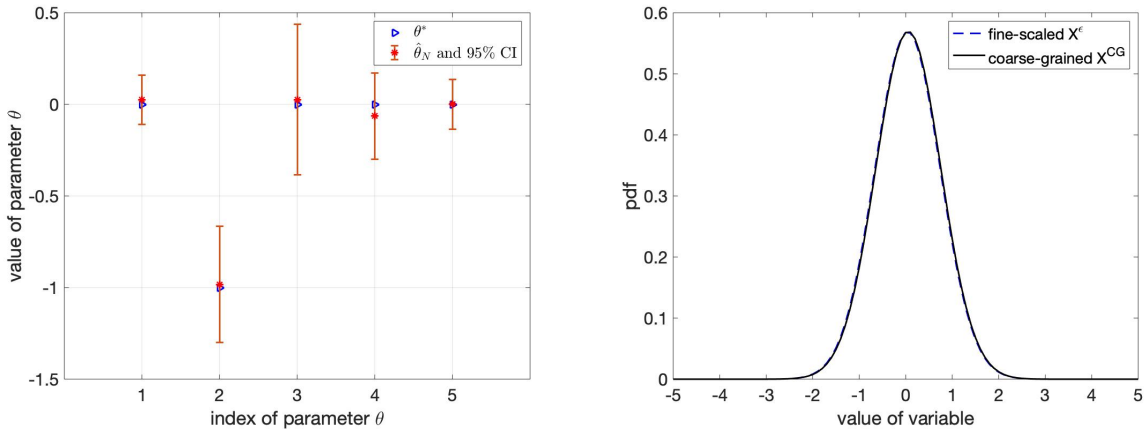


Figure 3: The left plot shows the results for Relative Entropy minimization. The density of CG variable matches well the one of X^ϵ .

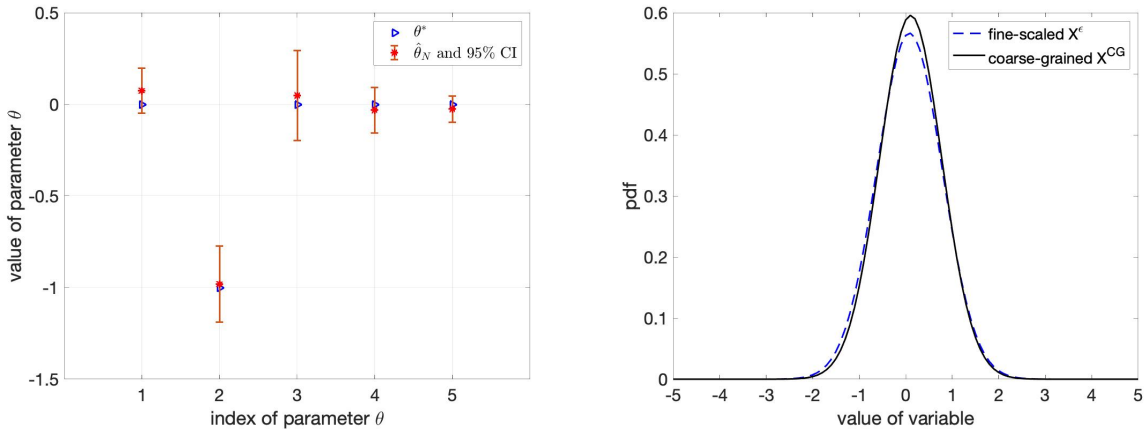


Figure 4: Path-space optimization with the RER method.

time-series data, $N_p = 1, N_t = 50,000$, and $N_p = 100, N_t = 500$. In all results presented next, the number of bootstrap samples is $B = 200$.

We compare the RE and FM estimates and confidence intervals for the sets of $N = 50$, $N = 200$ and $N = 500$, see table 3. For better readability we report results only for the parameter θ_2 . The complete table is given the supplementary information. Moreover, in the supplementary information, we report the parameter estimates and the asymptotic, jackknife, and bootstrap variance estimates obtained with the FM method for $N = 50, 100$, and 200 .

First, we notice that the jackknife estimate for the RE gives an inconsistent value of variance, thus making the confidence intervals too wide and useless. This is a common issue for the jackknife method with leaving one observation out each time, especially for non-smooth estimators. This well-known deficiency can be rectified by using a more general jackknife with leaving $d > 1$ observations out, [47], but with an extremely large computational cost, as it is common to choose $d = \sqrt{N}$. For example, with sample size $N = 50$ the jackknife with leaving $d = \sqrt{N} \approx 7$ observations out we need to compute 10^9 jackknife estimates which is impracticable even for this toy example.

N		Asymptotic with FM	Jackknife with FM	Bootstrap with FM	Asymptotic with RE	Jackknife with RE	Bootstrap with RE
50	$\hat{\theta}_2$		-0.8575			-0.8720	
	$\hat{\sigma}^2$	0.0654	0.0968	0.0982	0.0156	0.5296	0.0099
	CI	[-1.3589 -0.3562]	[-1.4674 -0.2477]	[-1.4717 -0.2433]	[-1.1165 -0.6275]	[-2.2984 0.5543]	[-1.0670 -0.6771]
200	$\hat{\theta}_2$		-0.9702			-0.9759	
	$\hat{\sigma}^2$	0.0167	0.0200	0.0197	0.0206	1.0325	0.0081
	CI	[-1.2233 -0.7172]	[-1.2476 -0.6929]	[-1.2452 -0.6953]	[-1.2574 -0.6945]	[-2.9675 1.0157]	[-1.1523 -0.7996]
500	$\hat{\theta}_2$		-1.0240			-0.9827	
	$\hat{\sigma}^2$	0.0063	0.0072	0.0069	0.0140	2.8518	0.0069
	CI	[-1.1790 -0.8689]	[-1.1900 -0.8579]	[-1.1868 -0.8611]	[-1.2287 -0.7505]	[-4.2963 2.3272]	[-1.1491 -0.8200]

Table 3: Comparison of the FM and RE methods and the corresponding asymptotic, jackknife, and bootstrap, variance σ^2 and 95% CIs, with i.i.d. samples.

Notice that the jackknife and bootstrap variances are slightly larger than the asymptotic variance. On the other hand, the jackknife and bootstrap variance estimates are very close for all cases. We observe also the improvement of the variance as the number of samples increases in all methods, as is expected. Despite the fact that the non-asymptotic and asymptotic variances here are comparable, the non-asymptotic approaches have advantages over standard asymptotic methods. Indeed, when the variance of the estimator does not admit an analytic formulation or is too complicated to calculate, the non-parametric methods are the only option. However, non-parametric methods have higher computational cost than the asymptotic due to the need for resampling and computing estimates repeatedly.

We calculate the bootstrap and jackknife estimates for the PSRE minimization, applied for multiple i.i.d. trajectories. With $N_p = 100$ trajectories, and $N_t = 300$ correlated samples in each trajectory, the 95% standard confidence intervals are reported in table 4. We also validate the accuracy of jackknife and bootstrap CI for the RER minimization, by computing confidence intervals with different sets of samples. On average, 94% Jackknife CIs and 94.8% Bootstrap CIs include the true values of the parameters θ^* .

Figure 5 presents the induced bootstrap confidence intervals for the drift as the QoI $a(x, \hat{\theta})$, computed by the corresponding quantiles of the set $\{a(x, \hat{\theta}_i)\}_{i=1}^B$, following (26). We observe that for only $N = 50$ samples the bootstrap confidence interval captures the 'large sample' ($N = 500$ in FM and RE, $N = 50000$ in RER) parameter estimates for all values of x . Note though, that the CI is wider for larger absolute values of x which depicts a wider uncertainty in the estimate.

V. Validation of confidence intervals. In the previews sections we estimated the asymptotic confidence intervals for i.i.d. data and time-series data. Table 5 shows the experiment results on

N_p	N_t	$\hat{\theta}$	Asymptotic CI	Jackknife CI	Bootstrap CI
1	50,000	$\begin{bmatrix} 0.0746 \\ -0.9805 \\ 0.0483 \\ -0.0313 \\ -0.0255 \end{bmatrix}$	$\begin{bmatrix} -0.0491 & 0.1983 \\ -1.1876 & -0.7733 \\ -0.1979 & 0.2944 \\ -0.1550 & 0.0925 \\ -0.0965 & 0.0455 \end{bmatrix}$	NA	NA
100	300	$\begin{bmatrix} -0.0807 \\ -0.9358 \\ 0.0270 \\ -0.0546 \\ 0.0169 \end{bmatrix}$	NA	$\begin{bmatrix} -0.2546 & 0.0932 \\ -1.1718 & -0.6997 \\ -0.4219 & 0.4759 \\ -0.1722 & 0.0630 \\ -0.1009 & 0.1346 \end{bmatrix}$	$\begin{bmatrix} -0.2498 & 0.0884 \\ -1.1897 & -0.6818 \\ -0.3791 & 0.4331 \\ -0.1928 & 0.0836 \\ -0.0939 & 0.1276 \end{bmatrix}$

Table 4: Jackknife and bootstrap 95% CI by RER on correlated data with multiple trajectories. NA means that the CI does not apply to that type of data.

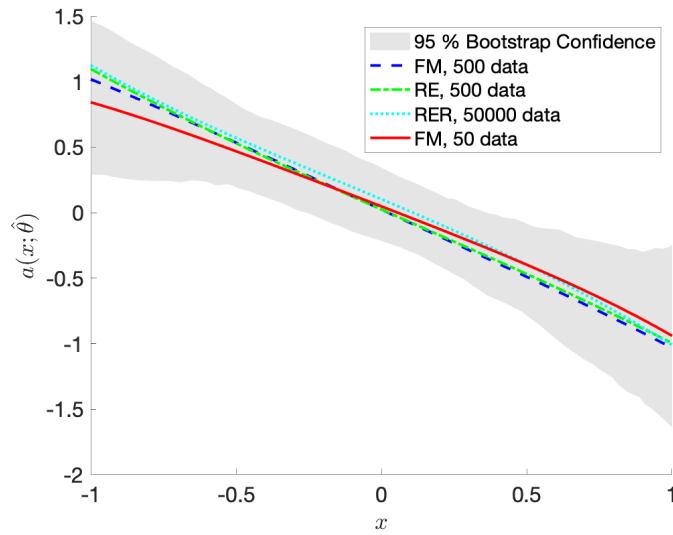


Figure 5: Drift function $a(x; \hat{\theta})$ with $\hat{\theta}$ estimated by different methods and 95% bootstrap percentile confidence interval. The number of bootstrap samples is 200.

validating those confidence intervals. For each method, sample size, and confidence level we calculate the corresponding confidence intervals for 500 independent sets of synthetic samples generated from (27). Then, we calculate the percentage of those confidence intervals containing the true value of the parameters. Those probabilities are close to the confidence levels, with RER’s probability being slightly smaller than the confidence level.

Method	Sample size	90% CI	95% CI	99% CI
FM	50	89.40%	93.84%	98.28%
FM	500	90.16%	95.68 %	98.88%
FM	5,000	87.56 %	92.96 %	98.56 %
RER	5,000	87.76 %	92.80 %	97.56 %
RER	50,000	88.00%	93.84 %	98.76%

Table 5: The percentage of the estimated confidence intervals that include the true values of the parameters. The percentage presented is the average over the corresponding percentages of the parameters.

5 Test-bed 2: Effective force-fields and confidence in coarse-graining of linear polymer chains

In the present section, we apply the methodology described in section 3 on the CG approximation of a polyethylene bulk system. Specifically, we derive effective force fields with the FM method and the corresponding confidence intervals. Our focus is to understand the behavior of the output model when the available data is limited. Thus, we concentrate on the non-asymptotic methods of section 3.2.

To generate the simulated data sets \mathcal{D}_N of i.i.d. configurations, Molecular Dynamics (MD) simulations of a united-atom polyethylene (PE) system were performed using home made (parallel) MD code. A PE chain is represented via a united-atom model in which each methylene CH_2 and methyl CH_3 group are considered as a single Van der Waals interacting site. Details of the model parameters are given in the supplementary information. The model system consists of 96 polyethylene chains of 99 monomer units ($-CH_2-$), i.e., the number of atomistic degrees of freedom is $n = 9504$. The simulations were performed under NVT conditions at temperature $T = 450$ K, and density $\rho = 0.76868$ gr/cm³. The integration time step was 2 fs. We record system configurations every 50 ps for about 500 ns = 500,000 ps. Thus, the size of the available data set is 10,000 (number of configurations). In the following, results are reported for a large $N = 2,000$ and smaller ($N = 200, 100, 30$) data sets, to examine the dependence of the predictions on the size of the actual data set. Note that we choose N_k configurations from the 10,000 to be equidistant, e.g., the configurations for the set $N = 2,000$ have distance $(10,000/2,000) * 50$ ps = 250 ps, and for $N = 200$ the distance is $(10,000/200) * 50$ ps = 2,500 ps. We should also note that the maximum relaxation time of the polymer chains is around 1,700 ps, calculated by fitting the end-to-end vector autocorrelation function using a stretched exponential. This suggests that the large set ($N = 2,000$) is composed of correlated data while the smaller ones ($N = 200, 100, 30$) are uncorrelated.

For the coarse-grained representation of the PE, we consider a 3 : 1 mapping representation, i.e., three monomer units form one CG particle, see figure 6. Thus, the total number of CG particles in the system is $m = 33 \times 96 = 3168$.

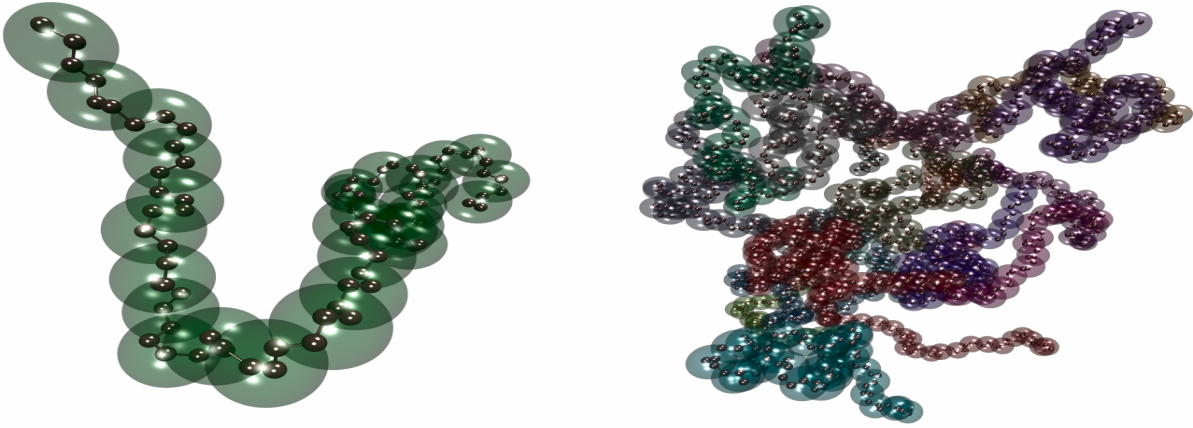


Figure 6: Snapshot of model polyethylene bulk system, shown in atomistic and CG (3:1 mapping scheme) description: a) single PE chain, b) PE bulk system.

The CG PE model exhibits both bonded and non-bonded interactions. First, we estimate all the CG interactions with the Iterative Inverse Boltzmann (IBI)[43] method, both non-bonded and bonded interactions (bonds, angles, dihedrals) presented in a tabulated form. We disregard the non-bonded estimates and keep only the bonded ones which are input for the FM method applied next. The resulting interaction potentials are reported in the supplementary information. Then, we estimate the non-bonded interactions with the FM method. We represent the non-bonded interactions with a two-body pair potential, which only depends on the distance between monomers. That is, the proposed CG potential described in Eq. (3) is

$$\bar{U}(\bar{\mathbf{q}}; \theta) = \sum_{I=1}^m \sum_{J \neq I}^m u(r; \theta),$$

where $r = |\bar{q}_I - \bar{q}_J|$. The CG pair interaction potential $u(r; \theta)$ is approximated via a functional basis of the form:

$$u(r; \theta) = \sum_{k=1}^K \theta_k \phi_k(r),$$

using the linear or the cubic B-splines $\{\phi_k(r)\}_{k=1}^K$, [41]. The cutoff range for the non-bonded interactions is 1.4 nm. The size of the parameter set θ is determined by the number of knots K . We present results for a varying number of (a) parameters K and (b) all-atom configurations N , given in table 6.

The QoI is the pair potential $u(r; \theta)$, $r > 0$, with estimator the random variable in \mathbb{R}

$$\hat{u}_N(r; \theta) = \sum_{k=1}^K \hat{\theta}_{k,N} \phi_k(r), \quad (37)$$

that is a linear combination of the parameter estimators $\hat{\theta}_N$.

For each combination of parameters and data set size, we find the optimal force field with the FM method. For the small data sets, we also derive the bootstrap and jackknife statistics for

the parameters. Next, we report the results for the cubic B-splines representation with $K = 30$ parameters. The results for the linear B-splines and comparisons between the different functional basis are reported in the supplementary information. In the results reported below, the number of bootstrap samples is $B = 200$. We consider the large data set ($N = 2,000$) estimation as a reliable approximation, and thus we use it as *reference* result to compare to estimations with the small data sets.

Figure 8 (a) depicts the parameters $\hat{\theta}_N$ estimated with the large ($N = 2,000$) and the small ($N = 200$) data set, along with the 95% bootstrap percentile CI. In figure 8 (b) we report the relative standard deviation (RSTD) of each nonzero parameter, defined by $\text{RSTD} = \hat{\sigma}_k / \hat{\theta}_k$, where $\hat{\sigma}_k$ is the standard deviation estimated with the bootstrap method. The RSTD reveals the most uncertain parameters, e.g., the spline parameters with index 12, 20, 23, 26, 29. We compare the asymptotic and bootstrap standard deviation $\hat{\sigma}$ in figure 7 for the $N = 30$ and $N = 200$ configurations. It is evident that the asymptotic and bootstrap variance differ for the $N = 30$ but are very close when $N = 200$.

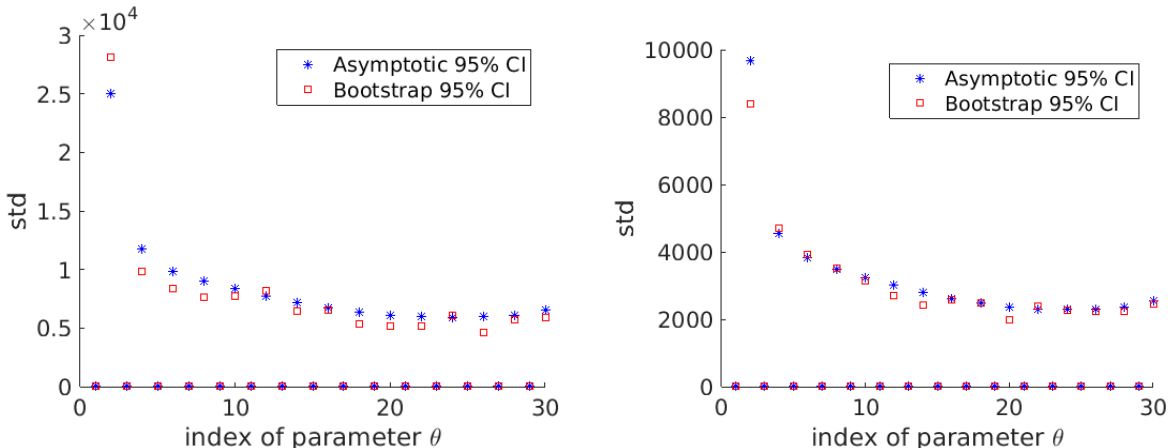


Figure 7: Asymptotic and bootstrap estimated standard deviation for $N = 30$ (left figure) and $N = 200$ (right figure) configurations.

Figure 9 depicts the small data set, $N = 200$, estimated pair potential, as well as the 80%, 95% and 99% bootstrap percentile confidence intervals. We observe that the estimated potential captures the minimum value point of the reference, though there is an amplitude deviation. Most importantly, the reference potential falls inside the 95% and 99% bootstrap CI for the whole range of distances. This observation suggests that for $N = 200$, the bootstrap CI is capable of providing useful information for the range and minima of the potential.

In order to examine the dependence of the CG potential on the size of the data set, we present in Figure 10 the resulting effective potential of CG PE beads, as well as its 95% CI, analyzing an increasing number of atomistic configurations. We observe that the CI for $N = 30$ is practically uninformative, as its range is too wide.

Next, we examine the bootstrap standard deviation (STD) of the CG pair potential values, as a function of the CG beads distance. Results for the bootstrap STD are shown in Figure 11, evaluated for varying number of configurations. Two useful observations can be made out of these data. First, it is interesting that the STD decreases with increasing the potential interaction range, i.e., the distance between CG particles, for all cases. Indeed, the most uncertain values of the CG pair potential are for small distances. This is not surprising if we consider that at larger distances the configurations are more 'homogeneous' (pair distribution function approaches one), and thus

	Number of parameters	Small data set size	Large data set size
Linear	75	300	5000
	30	200	2000
Cubic	30	30	2000
		100	
		200	

Table 6: Available sample sets for the PE model.

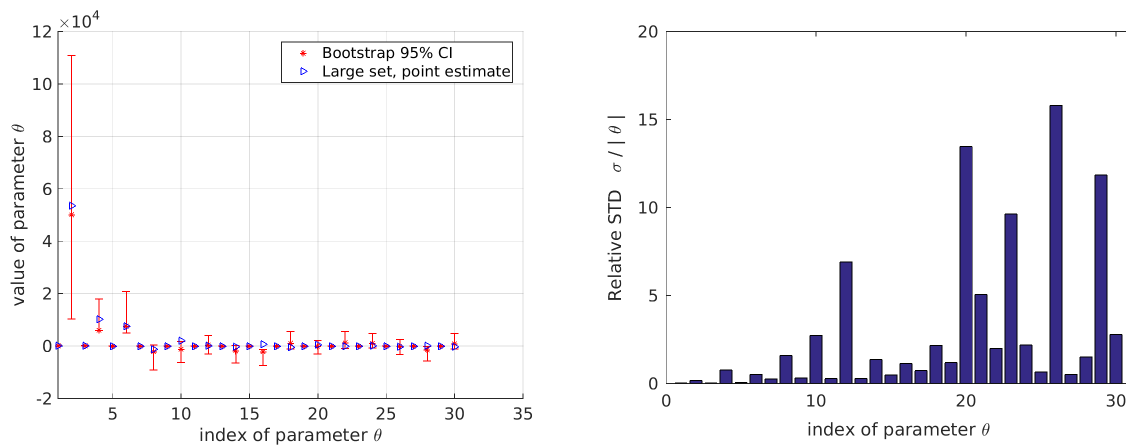


Figure 8: CG PE effective potential: (a) Small sample ($N = 200$) parameter estimate, and bootstrap 95% CI. (b) Relative standard deviation of the parameters, reveals the most uncertain parameters.

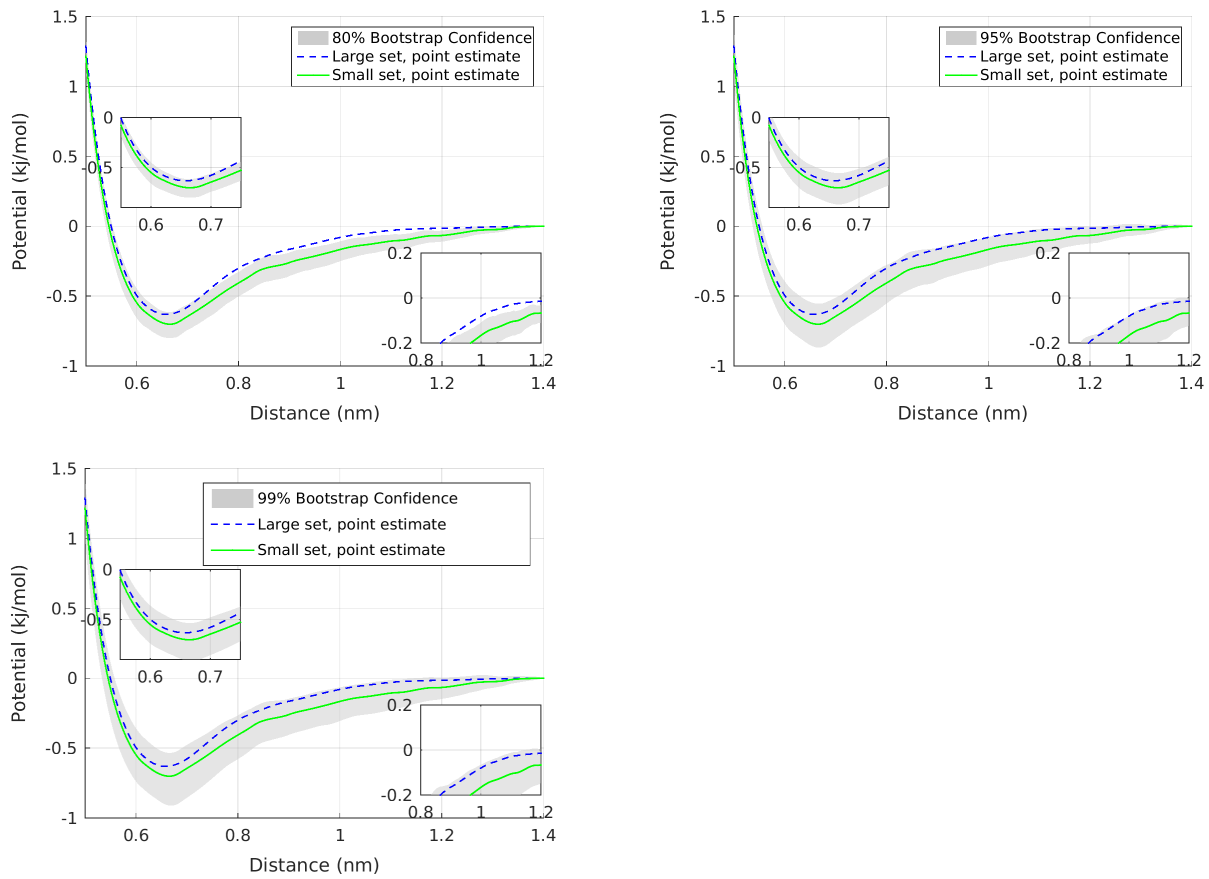


Figure 9: Estimated CG PE pair interaction potential $\hat{u}(r)$ for a large (2000) and a small (200) data set, and the 80%, 95%, and 99% bootstrap percentile CI.

the variance is expected to be smaller. Second, the STD decreases with increasing the number of configurations, and the deviation between them is lower as the data set increases. Thus, given a desired accuracy, the STD can serve as a criterion for choosing a sufficient number of configurations.

The 95% jackknife CI for the CG PE pair potential is presented in figure 12, for $N = 200$. It is clear that the jackknife CI can also capture the reference potential for this size of the data set.

Furthermore, to examine the CG interaction potential predictions at specific particle distances, the mean, the standard deviation, and the percentile CI values are shown in Figure 13 and in tables 7, 8 and 9 for three distances $r = 0.45, 0.65, 0.95$. In more detail, Figure 13 and table 7 depict the estimate and CI for the pair potential at distance $r = 0.65$ nm for various data sets. This distance corresponds to the reference potential minimum (see also Figure 8, 9). It is clear to see the change of the probability density, and the most probable CG potential value, with the increase of the data set size. Indeed, as the size of the available configurations change from 30 up to 200 a 'concentration of the density' is also observed. At the same time, the expected (average) value approaches the one of the underlying reference system ($N = 2,000$), shown in table 7.

Qualitatively similar are the results for the other two distances $r = 0.45$ nm, which is in the repulsive part of the potential, and $r = 0.95$ nm that is in the attractive 'tail', shown in tables 8 and 9 respectively. For both distances, the bootstrap predictions become more accurate (CIs are reduces) as the size of the data set increases. For $N = 200$ the bootstrap and jackknife predictions are very similar.

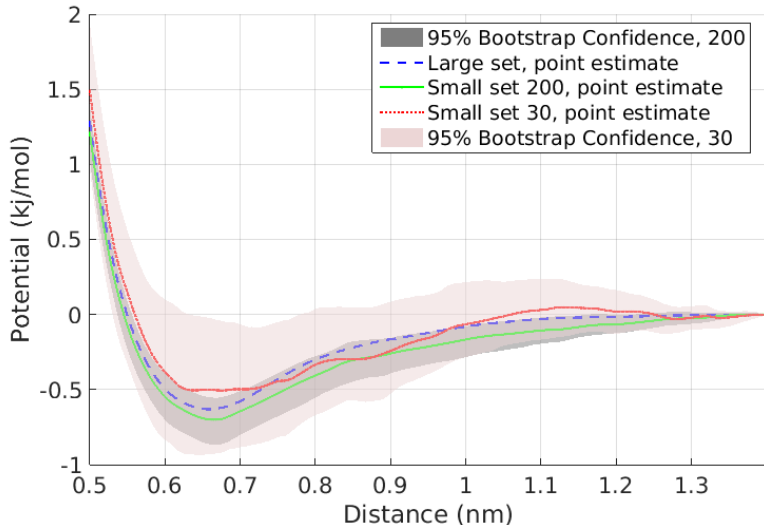


Figure 10: 95% bootstrap CI of the CG PE pair effective potentials, for two small data sets, $N = 200$ and 30 configurations.

As a final check, and in order to understand the effect of the autocorrelated data on the effective model we present in figure 14 the pair potential point estimates obtained by the FM method with (a) a set of 200 correlated configurations with distance $\tau = 50$ ps, (b) the reference large set of $N = 2,000$ configurations with distance $\tau = 250$ ps and and (c) the set of $N = 200$ uncorrelated configurations with distance $\tau = 2,500$ ps. Recall, that the estimated relaxation time is 1,700 ps.

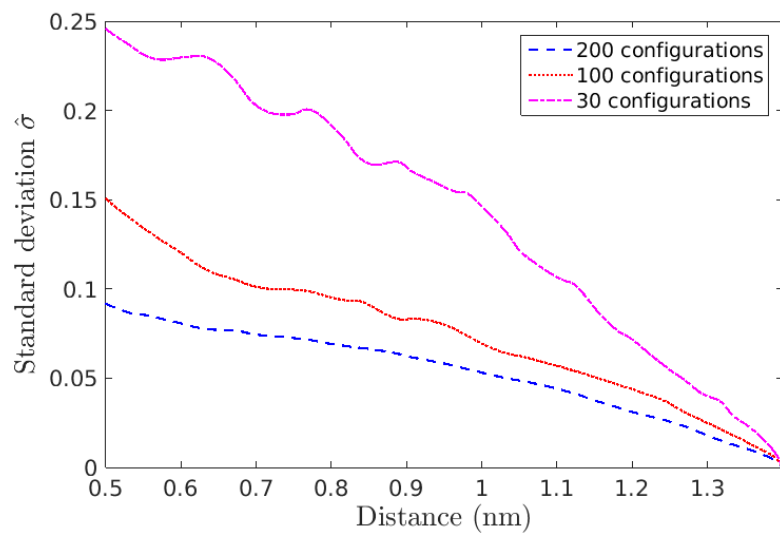


Figure 11: Bootstrap standard deviation of the CG PE pair effective potentials for the data sets of 200, 100, and 30 configurations.

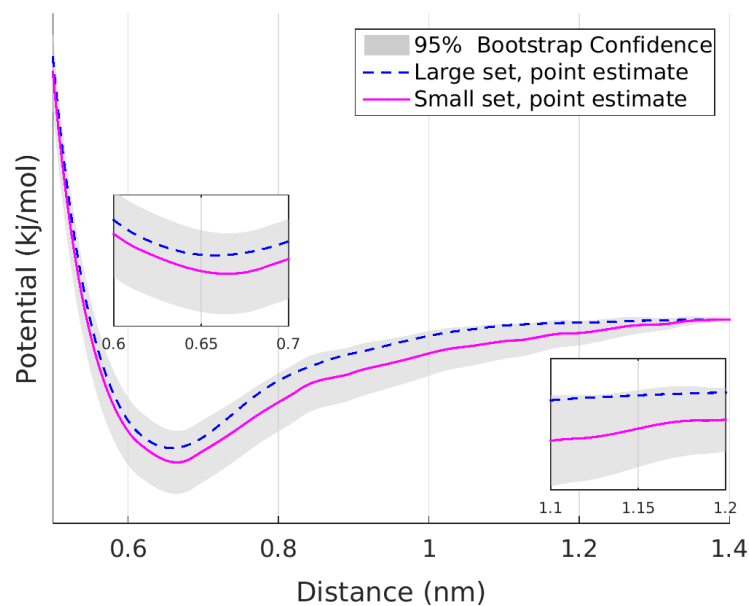


Figure 12: The jackknife 95% CI for the estimated CG PE pair effective interaction potential $u(r)$, for the $N = 200$ configurations data set.

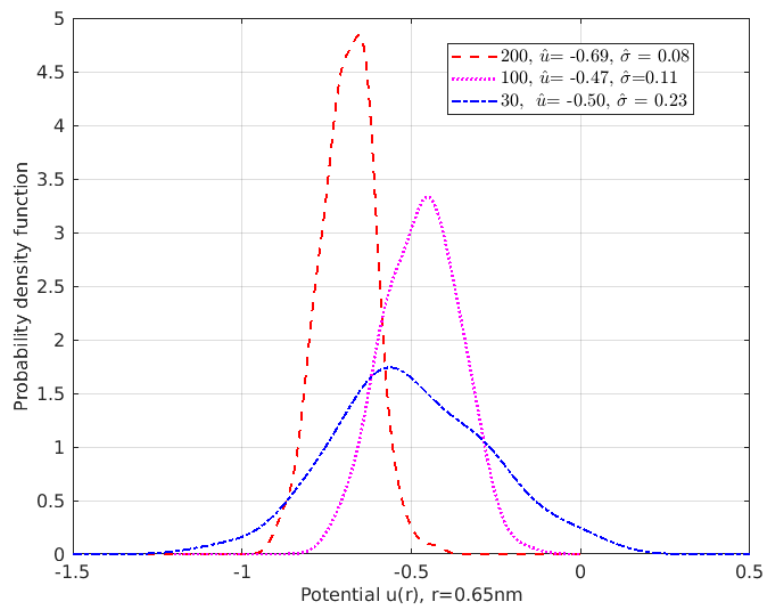


Figure 13: Probability density function of CG PE pair effective potential $u(r)$, at $r = 0.65\text{nm}$, derived from bootstrap, for three small data sets involving 200, 100, and 30 atomistic configurations. The corresponding reference value is $\hat{u} = -0.6289$.

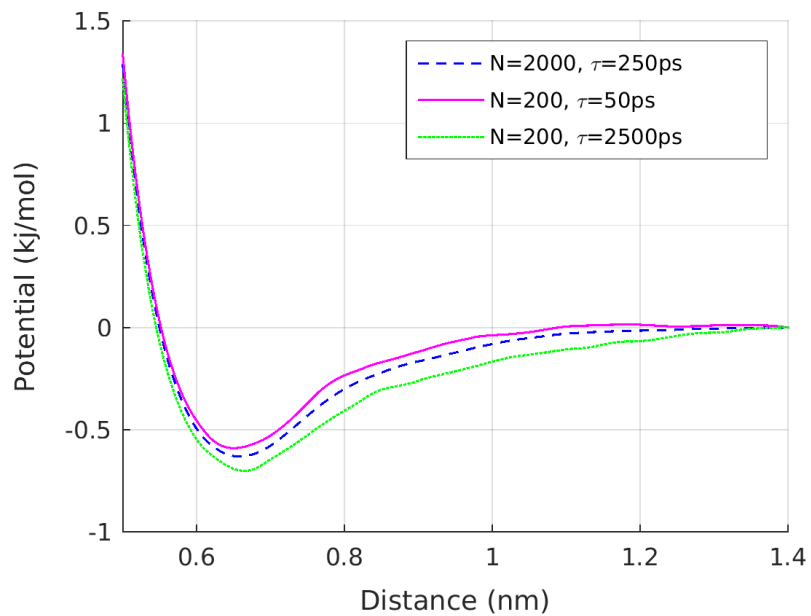


Figure 14: FM estimates for correlated and uncorrelated data.

Method	\hat{u}	$\hat{\sigma}_u$	CI	Number of samples
Large data set	-0.6289			2000
Bootstrap	-0.5027	0.2259	(-0.9343, -0.0145)	30
	-0.4706	0.1079	(-0.6847, -0.2796)	100
	-0.6900	0.0770	(-0.8504, -0.5417)	200
Jackknife	-0.6900	0.0794	(-0.8463, -0.5348)	200

Table 7: Mean, standard deviation, and percentile CI for $u(r)$, $r = 0.65$

Method	\hat{u}	$\hat{\sigma}_u$	CI	Number of samples
Large data set	4.3263			2000
Bootstrap	4.5663	0.2896	(3.9611, 5.1605)	30
	4.3743	0.1716	(4.0619, 4.6749)	100
	4.2631	0.1036	(4.0542, 4.4686)	200
Jackknife	4.2631	0.1078	(4.0522, 4.4748)	200

Table 8: Mean, standard deviation, and percentile CI for $u(r)$, $r=0.45$

6 Guidelines and Discussion

To conclude, in this work, we presented an array of methodologies to generate confidence intervals for systematic bottom-up coarse-grained models, derived from both equilibrium and path-space observations. The coarse-graining approach is physics and data driven, relating the true CG model to its digital-twin, the approximate CG model.

We have employed rigorous statistics theory tools for constructing asymptotic and non-asymptotic CIs, and examined their applicability to coarse-graining strategies. We present a schematic guideline in figure 15 for the methodology we propose. The main features of the methodology, as depicted in the schematic guideline and observed in the test-bed problems, are:

- Asymptotic vs. non-asymptotic: The asymptotic methods need a parametric form of the variance since we compute the expectation of the first and second derivatives of the log density or transition probability function. While the non-asymptotic methods do not need a parametric form of the variance, they have an additional computation cost due to the repeated optimization to compute sample estimates. Therefore, if an analytic form of variance can be derived, asymptotic methods are more computationally efficient.
- Time-series data vs. independent data: Independent data can provide more information as their statistical analysis is well established, but obtaining independent data in real-world problem is often impractical. Correlated data, such as time-series data, are more commonly used. Our proposed confidence intervals for the RER minimization, provides a useful uncertainty quantification of the estimated parameters for time-series data, under the assumption of stationary and ergodicity.
- Correlated data in multiple independent trajectories: we also demonstrated in table 4 that by using the independence between trajectories a resampling technique, jackknife and bootstrap, can also construct non-asymptotic confidence intervals for this type of data.

In short, we have demonstrated:

- the need for employing non-asymptotic methods in coarse-graining high dimensional molecular systems, and

Method	\hat{u}	$\hat{\sigma}_u$	CI	Number of samples
Large data set	-0.1210			2000
Bootstrap	-0.1488	0.1571	(-0.3974, 0.1313)	30
	0.0687	0.0799	(-0.0583, 0.2453)	100
	-0.2216	0.0582	(-0.3312, -0.1156)	200
Jackknife	-0.2138	0.0613	(-0.3339, -0.0937)	200

Table 9: Mean, standard deviation, and percentile CI for $u(r)$, $r=0.95$

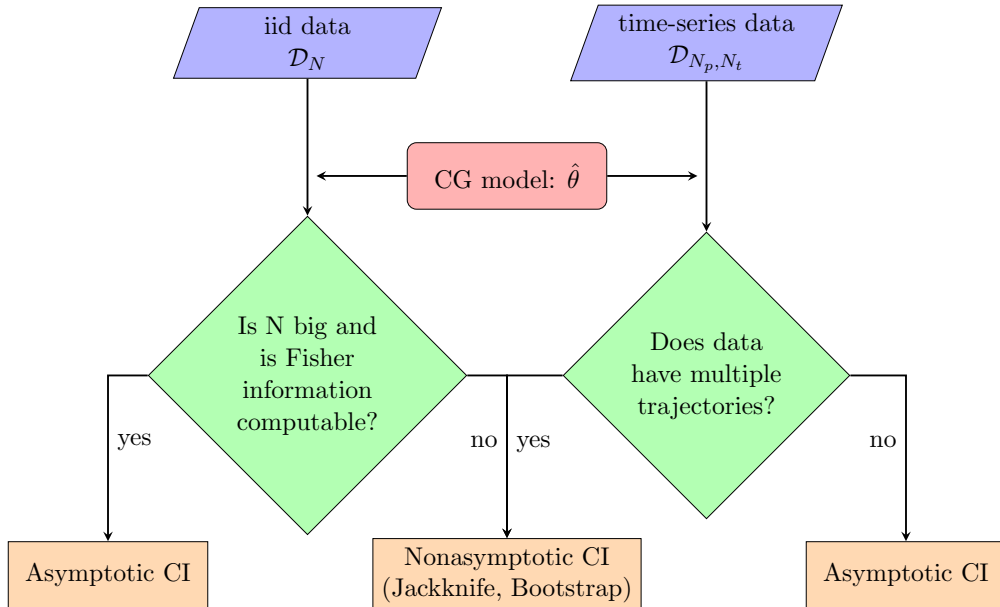


Figure 15: Schematic methodology for confidence interval estimation in coarse-graining

- the benefit of applying time series, path-space techniques.

As it is often extremely time-consuming to generate 'large' data sets of atomistic model configurations in molecular, and especially macromolecular systems, the asymptotic confidence intervals are often not valid. Therefore, we propose non-parametric, non-asymptotic methods, i.e., bootstrap and jackknife methods to provide guaranties of the coarse-grained output model in terms of the size of the available data.

Moreover, we show with the benchmark example that the path-space method, i.e., the RER optimization, is best in terms of the cost of generating simulated data, for which we can also provide confidence intervals. Also, the FM estimator for correlated data gives reliable point estimates though corresponding confidence sets cannot be obtained. Indeed, since the bottom-up CG methods are based on simulated data, often for high-dimensional systems, not discarding simulated data to achieve independence saves a large amount of computational time.

For the polymer melt, at realistic conditions, we have presented the bootstrap and jackknife confidence intervals for the FM estimated parameters and the pair potential. A detailed analysis of the CIs for the derived effective CG non-bonded potential suggests that the sufficiency of the data size can be estimated along with the estimated bootstrap variance.

We believe that our work could stimulate further studies on the development and application of rigorous statistical inference methods for coarse-grained models of soft condensed matter, and

in particular, of macromolecular systems. This is even more important for hybrid polymer-based complex materials, for which the relaxation times increase rapidly with the complexity of the underlying physico-chemical interactions, thus making the sampling of either a large number of atomistic i.i.d or long time-correlated configurations not feasible [5, 44].

Acknowledgements

The research of M.K. was partially supported by NSF TRIPODS CISE-1934846 and by the Air Force Office of Scientific Research (AFOSR) under the grant FA-9550-18-1-0214. The research of T. J. was partially supported by the National Science Foundation (NSF) under the grant DMS-1515712 and by the Air Force Office of Scientific Research (AFOSR) under the grant FA-9550-18-1-0214. E.K. acknowledges support by the Hellenic Foundation for Research and Innovation (HFRI) and the General Secretariat for Research and Technology (GSRT), under grant agreement No [52].

References

- [1] P. Angelikopoulos, C. Papadimitriou, and P. Koumoutsakos. Bayesian uncertainty quantification and propagation in molecular dynamics simulations: A high performance computing framework. *The Journal of Chemical Physics*, 137(14):144103, 2012.
- [2] P. Angelikopoulos, C. Papadimitriou, and P. Koumoutsakos. Data driven, predictive molecular dynamics for nanoscale flow simulations under uncertainty. *The Journal of Physical Chemistry B*, 117(47):14808–14816, 2013.
- [3] G. Casella and R.L. Berger. *Statistical Inference*. Duxbury advanced series in statistics and decision sciences. Thomson Learning, 2002.
- [4] A. Chaimovich and M. S. Shell. Anomalous waterlike behavior in spherically-symmetric water models optimized with the relative entropy. *Phys. Chem. Chem. Phys.*, 11:1901–1915, 2009.
- [5] P. Bačová, E. Glynos, S. Anastasiadis, and V. Harmandaris. Nanostructuring single-molecule polymeric nanoparticles via macromolecular architecture host. *ACS Nano*, 13:2439–2449, 2019.
- [6] Thomas J DiCiccio and Bradley Efron. Bootstrap confidence intervals. *Statistical science*, pages 189–212, 1996.
- [7] M. Doi and S.F. Edwards. *The Theory of Polymer Dynamics*. Clarendon Press, 1986.
- [8] P. Dupuis, M. A. Katsoulakis, Y. Pantazis, and P. Plecháč. Path-space information bounds for uncertainty quantification and sensitivity analysis of stochastic dynamics. *SIAM J. Uncert. Quant.*, 4(1):80–111, 2016.
- [9] R. Dutta, Z. F. Brotzakis, and A. Mira. Bayesian calibration of force-fields from experimental data: Tip4p water. *The Journal of Chemical Physics*, 149(15):154110, 2018.
- [10] B. Efron. Bootstrap methods: Another look at the jackknife. *Ann. Statist.*, 7(1):1–26, 01 1979.
- [11] B. Efron and T. Hastie. *Computer Age Statistical Inference*. Institute of Mathematical Statistics Monographs. Cambridge University Press, 2016.

- [12] K. Farrell, J. T. Oden, and D. Faghihi. A Bayesian framework for adaptive selection, calibration, and validation of coarse-grained models of atomistic systems. Journal of Computational Physics, 295:189 – 208, 2015.
- [13] K. Farrell-Maupin and J. T. Oden. Adaptive selection and validation of models of complex systems in the presence of uncertainty. Research in the Mathematical Sciences, 4(1):14, Aug 2017.
- [14] L. Felsberger and P.-S. Koutsourelakis. Physics-constrained, data-driven discovery of coarse-grained dynamics. Communications in Computational Physics, 25(5):1259–1301, 2019.
- [15] S. L. Frederiksen, K. W. Jacobsen, K. S. Brown, and J. P. Sethna. Bayesian ensemble approach to error estimation of interatomic potentials. Phys. Rev. Lett., 93:165501, Oct 2004.
- [16] M.I. Freidlin, J. Szucs, and A.D. Wentzell. Random Perturbations of Dynamical Systems. Grundlehren der mathematischen Wissenschaften. Springer New York, 2012.
- [17] Jerome Friedman, Trevor Hastie, and Robert Tibshirani. The elements of statistical learning, volume 1(10). Springer series in statistics New York, 2001.
- [18] V. Harmandaris, E. Kalligiannaki, and M. Katsoulakis. Computational Design of Complex Materials Using Information Theory: From Physics- to Data-driven Multi-scale Molecular Models. ERCIM News. Special theme: Digital Twins, 115, 2018.
- [19] V. Harmandaris, E. Kalligiannaki, M. Katsoulakis, and P. Plechac. Path-space variational inference for non-equilibrium coarse-grained systems. Journal of Computational Physics, 314:355 – 383, 2016.
- [20] V. Harmandaris and K. Kremer. Dynamics of polystyrene melts through hierarchical multiscale simulations. Macromolecules, 42:791, 2009.
- [21] V. Harmandaris and K. Kremer. Predicting polymer dynamics at multiple length and time scales. Soft Matter, 5:3920, 2009.
- [22] V. Harmandaris, V. G. Mavrantzas, D. Theodorou, M. Kröger, J. Ramírez, H.C. Öttinger, and D. Vlassopoulos. Dynamic crossover from rouse to entangled polymer melt regime: Signals from long, detailed atomistic molecular dynamics simulations, supported by rheological experiments. Macromolecules, 36:1376–1387, 2003.
- [23] S Izvekov and GA Voth. Effective force field for liquid hydrogen fluoride from ab initio molecular dynamics simulation using the force-matching method. The Journal of Physical Chemistry. B, 109(14):6573–6586, 04 2005.
- [24] S. Izvekov and G.A. Voth. Multiscale coarse graining of liquid-state systems. The Journal of Chemical Physics, 123(13):134105, 2005.
- [25] L. C. Jacobson, R. M. Kirby, and V. Molinero. How Short Is Too Short for the Interactions of a Water Potential? Exploring the Parameter Space of a Coarse-Grained Water Model Using Uncertainty Quantification. The Journal of Physical Chemistry B, 118(28):8190–8202, 2014.
- [26] G. L. Jones. On the Markov chain central limit theorem. Probability surveys, 1(299-320):5–1, 2004.

- [27] G. L Jones, M. Haran, B. S Caffo, and R. Neath. Fixed-width output analysis for Markov chain Monte Carlo. Journal of the American Statistical Association, 101(476):1537–1547, 2006.
- [28] M. A. Katsoulakis and P. Plechac. Information-theoretic tools for parametrized coarse-graining of non-equilibrium extended systems. J. Chem. Phys., 139:4852–4863, 2013.
- [29] M. A. Katsoulakis and P. Vilanova. Data-driven, variational model reduction of high-dimensional reaction networks. Journal of Computational Physics, 401:108997, 2020.
- [30] Pu L., Qiang S., Hal D., and Gregory A. Voth. A Bayesian statistics approach to multiscale coarse graining. The Journal of Chemical Physics, 129(21):214114, 2008.
- [31] S. Longbottom and P. Brommer. Uncertainty quantification for classical effective potentials: an extension to potfit. Modelling and Simulation in Materials Science and Engineering, 27(4):044001, 2019.
- [32] A.P. Lyubartsev and A. Laaksonen. Calculation of effective interaction potentials from radial distribution functions: A reverse Monte Carlo approach. Phys. Rev. E, 52:3730–3737, 1995.
- [33] A.P. Lyubartsev, A. Mirzoev, L. Chen, and A. Laaksonen. Systematic coarse-graining of molecular models by the newton inversion method. Faraday Discussion, 144(1):43–56, 2010.
- [34] R. G. Miller. The Jackknife—A Review. Biometrika, 61(1):1–15, 1974.
- [35] F. Müller-Plathe. Coarse-graining in polymer simulation: From the atomistic to the mesoscopic scale and back. ChemPhysChem, 3(9):754–769, 2002.
- [36] W. G. Noid. Systematic methods for structurally consistent coarse-grained models. Methods Mol. Biol., 924(9):487–531, 2013.
- [37] W. G. Noid, J. Chu, G.S. Ayton, V. Krishna, S. Izvekov, G.A. Voth, A. Das, and H.C. Andersen. The multiscale coarse-graining method. I. A rigorous bridge between atomistic and coarse-grained models. The Journal of Chemical Physics, 128(24):244114, 2008.
- [38] W. G. Noid, Jih-Wei Chu, Gary S. Ayton, and Gregory A. Voth. Multiscale coarse-graining and structural correlations: Connections to liquid-state theory. The Journal of Physical Chemistry B, 111(16):4116–4127, 2007.
- [39] W. G. Noid, P. Liu, Y. Wang, J. Chu, G.S. Ayton S. Izvekov, H.C. Andersen, and G.A. Voth. The multiscale coarse-graining method. II. Numerical implementation for coarse-grained molecular models. The Journal of Chemical Physics, 128(24):244115, 2008.
- [40] B. Oksendal. Stochastic Differential Equations: An Introduction with Applications. Hochschul-text / Universitext. U.S. Government Printing Office, 2003.
- [41] W.H. Press, S.A. Teukolsky, W.T. Vetterling, and B.P. Flannery. Numerical Recipes. Cambridge University Press, 2007.
- [42] J. Proppe and M. Reiher. Reliable estimation of prediction uncertainty for physicochemical property models. Journal of Chemical Theory and Computation, 13(7):3297–3317, 2017. PMID: 28581746.
- [43] D. Reith, M. Pütz, and F. Müller-Plathe. Deriving effective mesoscale potentials from atomistic simulations. Journal of Computational Chemistry, 24(13):1624–1636, 2003.

- [44] A. Rissanou, P. Bačová, and V. Harmandaris. Investigation of the properties of nanographene in polymer nanocomposites through molecular simulations: Dynamics and anisotropic brownian motion. PCCP, 21:23843–23854, 2019.
- [45] J. F. Rudzinski. Recent progress towards chemically-specific coarse-grained simulation models with consistent dynamical properties. Computation, 7(3), 2019.
- [46] M. Schöberl, N. Zabaras, and P.-S. Koutsourelakis. Predictive coarse-graining. Journal of Computational Physics, 333:49 – 77, 2017.
- [47] Jun Shao and CF Jeff Wu. A general theory for jackknife variance estimation. The Annals of Statistics, pages 1176–1197, 1989.
- [48] M.S. Shell. The relative entropy is fundamental to multiscale and inverse thermodynamic problems. The Journal of Chemical Physics, 129(14):–, 2008.
- [49] W. Tschöp, K. Kremer, O. Hahn, J. Batoulis, and T. Bürger. Simulation of polymer melts. I. coarse-graining procedure for polycarbonates. Acta Polym., 49:61, 1998.
- [50] A. Tsourtis, V. Harmandaris, and D. Tsagkarogiannis. Parameterization of coarse-grained molecular interactions through potential of mean force calculations and cluster expansions techniques. Entropy, 19:395, 2017.
- [51] A. Tsourtis, Y. Pantazis, M. Katsoulakis, and V. Harmandaris. Parametric sensitivity analysis for stochastic molecular systems using information theoretic metrics. The Journal of Chemical Physics, 143:014116, 2015.
- [52] L. Wasserman. All of nonparametric statistics. Springer Science & Business Media, 2006.
- [53] L. Wasserman. All of Statistics: A Concise Course in Statistical Inference. Springer Texts in Statistics. Springer New York, 2010.
- [54] T. Weymuth, J. Proppe, and M. Reiher. Statistical analysis of semiclassical dispersion corrections. Journal of Chemical Theory and Computation, 14(5):2480–2494, 2018.

Supplementary Information: Data-driven Uncertainty Quantification for Systematic Coarse-grained Models

1 Asymptotic convergence results

1.1 Asymptotic theorem for i.i.d. data

Suppose we have N i.i.d. fine-scale data

$$X_1, X_2, \dots, X_N,$$

where $X_i \in \mathcal{M} = \mathbb{R}^D$, $i = 1, \dots, N$. Assume that fine-scale data is distributed with probability density $p(x)$.

The coarse-graining (CG) map Π is defined as

$$\Pi : \mathcal{M} \rightarrow \mathcal{M}_{CG},$$

where $\mathcal{M}_{CG} = \mathbb{R}^d$, $d \ll D$. Note that the CG map Π is surjective here, that is, $\Pi^{-1}(\mathcal{M}_{CG}) = \mathcal{M}$.

Let us assume that the parametric family of the CG models \mathcal{Q}^θ has probability density q^θ . We obtain the optimal CG model by minimizing the relative entropy

$$\mathcal{R}(p|q^\theta \circ \Pi) := \mathbb{E}_p \left[\log \frac{p(X)}{q^\theta \circ \Pi(X)} \right]. \quad (1)$$

In addition, we have $\mathcal{R}(p|q^\theta \circ \Pi) = \lim_{N \rightarrow \infty} \hat{R}_N(p|q^\theta \circ \Pi)$ where

$$\hat{R}_N(p|q^\theta \circ \Pi) := \frac{1}{N} \sum_{i=1}^N \log \frac{p(X_i)}{q^\theta \circ \Pi(X_i)}. \quad (2)$$

Thus, the minimization of RE (1) is asymptotically equivalent to the optimization problem

$$\min_{\theta} \hat{R}_N(p|q^\theta \circ \Pi) \Leftrightarrow \max_{\theta} \frac{1}{N} \sum_{i=1}^N \log \left(q^\theta \circ \Pi(X_i) \right).$$

Let's also define

$$\ell_N(\theta) := \frac{1}{N} \sum_{i=1}^N \log \left(q^\theta \circ \Pi(X_i) \right),$$

$$\theta^* := \arg \min_{\theta} \mathcal{R}(p|q^\theta \circ \Pi),$$

$$\hat{\theta}_N := \arg \max_{\theta} \frac{1}{N} \sum_{i=1}^N \log \left(q^\theta \circ \Pi(X_i) \right).$$

Corollary 1.1.1.

$$\mathbb{E}_p[\nabla_{\theta} \log q^\theta \circ \Pi(X)|_{\theta=\theta^*}] = \vec{0}.$$

Proof. By the definition of θ^* , the gradient of $\mathcal{R}(p|q^\theta \circ \Pi)$ equals to $\vec{0}$ at $\theta = \theta^*$. Therefore, $\nabla_{\theta} \mathcal{R}(p|q^\theta \circ \Pi) = \nabla_{\theta} \mathbb{E}_p[\log q^\theta \circ \Pi(X)|_{\theta=\theta^*}] = 0$. The fact that $\mathbb{E}_p[\nabla_{\theta} \log q^\theta \circ \Pi(X)|_{\theta=\theta^*}] = \nabla_{\theta} \mathbb{E}_p[\log q^\theta \circ \Pi(X)|_{\theta=\theta^*}]$ yields the result. \square

Let \xrightarrow{P} denote convergence in probability. We say $\hat{\theta}_n \xrightarrow{P} \theta^*$ if, for every $\epsilon > 0$,

$$P(|\hat{\theta}_N - \theta^*| > \epsilon) \rightarrow 0 \quad \text{as } N \rightarrow \infty.$$

Corollary 1.1.2. (*Consistency of the estimator*) Suppose that

$$\sup_{\theta} |\hat{R}_N(p|q^\theta \circ \Pi) - R(p|q^\theta \circ \Pi)| \xrightarrow{P} 0,$$

and that, for every $\epsilon > 0$,

$$\inf_{\theta: |\theta - \theta^*| > \epsilon} R(p|q^\theta \circ \Pi) > R(p|q^{\theta^*} \circ \Pi).$$

Then

$$\hat{\theta}_N \xrightarrow{P} \theta^* \quad \text{as } N \rightarrow \infty$$

Proof. Since θ^* minimizes $R(p|q^\theta \circ \Pi)$, so $R(p|q^{\theta^*} \circ \Pi) \leq R(p|q^{\hat{\theta}_N} \circ \Pi)$.

$$\begin{aligned} R(p|q^{\hat{\theta}_N} \circ \Pi) - R(p|q^{\theta^*} \circ \Pi) &= R(p|q^{\hat{\theta}_N} \circ \Pi) - \hat{R}_N(p|q^{\theta^*} \circ \Pi) + \hat{R}_N(p|q^{\theta^*} \circ \Pi) - R(p|q^{\theta^*} \circ \Pi) \\ &\leq R(p|q^{\hat{\theta}_N} \circ \Pi) - \hat{R}_N(p|q^{\hat{\theta}_N} \circ \Pi) + \hat{R}_N(p|q^{\theta^*} \circ \Pi) - R(p|q^{\theta^*} \circ \Pi) \\ &\leq \sup_{\theta} |R(p|q^{\hat{\theta}_N} \circ \Pi) - \hat{R}_N(p|q^{\hat{\theta}_N} \circ \Pi)| + \hat{R}_N(p|q^{\theta^*} \circ \Pi) - R(p|q^{\theta^*} \circ \Pi) \\ &\xrightarrow{P} 0, \end{aligned}$$

where the first inequality follows from $\hat{R}_N(p|q^{\theta^*} \circ \Pi) \geq \hat{R}_N(p|q^{\hat{\theta}_N} \circ \Pi)$, and the last line follows from the first assumption. Hence for any $\delta > 0$, we have

$$P(R(p|q^{\hat{\theta}_N} \circ \Pi) > R(p|q^{\theta^*} \circ \Pi) + \delta) \rightarrow 0.$$

By the second assumption, for any $\epsilon > 0$, there exists $\delta > 0$ such that $|\theta - \theta^*| > \epsilon$ implies $R(p|q^\theta \circ \Pi) > R(p|q^{\theta^*} \circ \Pi) + \delta$, hence

$$P(|\hat{\theta}_N - \theta^*| > \epsilon) \leq P(R(p|q^{\hat{\theta}_N} \circ \Pi) > R(p|q^{\theta^*} \circ \Pi) + \delta) \rightarrow 0,$$

yields the consistency of the estimator. \square

The Fisher information matrices are defined as

$$\mathcal{F}_1(\theta^*) := -\mathbb{E}_p[\nabla_\theta^2 \log q^\theta \circ \Pi(X)|_{\theta=\theta^*}], \quad (3a)$$

$$\mathcal{F}_2(\theta^*) := \mathbb{E}_p[(\nabla_\theta \log q^\theta \circ \Pi(X))(\nabla_\theta \log q^\theta \circ \Pi(X))^{tr}|_{\theta=\theta^*}]. \quad (3b)$$

Here \cdot^{tr} denotes matrix transpose.

Corollary 1.1.3. *If $p = q^{\theta^*} \circ \Pi$, then*

$$\mathcal{F}_1(\theta^*) = \mathcal{F}_2(\theta^*).$$

Proof.

$$-\nabla_\theta^2 \log q^\theta \circ \Pi(X) = (\nabla_\theta \log q^\theta \circ \Pi(X))(\nabla_\theta \log q^\theta \circ \Pi(X))^{tr} - \frac{\nabla_\theta^2 q^\theta \circ \Pi(X)}{q^\theta \circ \Pi(X)}.$$

Take expectation with respect to the measure p at $\theta = \theta^*$ on both sides, yields,

$$\mathcal{F}_1(\theta^*) = \mathcal{F}_2(\theta^*) - \mathbb{E}_p \left[\frac{\nabla_{\theta}^2 q^{\theta} \circ \Pi(X)}{q^{\theta} \circ \Pi(X)} \Big|_{\theta=\theta^*} \right].$$

If $p = q^{\theta^*} \circ \Pi$, the last term

$$\begin{aligned} \mathbb{E}_p \left[\frac{\nabla_{\theta}^2 q^{\theta} \circ \Pi(X)}{q^{\theta} \circ \Pi(X)} \Big|_{\theta=\theta^*} \right] &= \int \frac{\nabla_{\theta}^2 q^{\theta^*} \circ \Pi(X)}{q^{\theta^*} \circ \Pi(X)} q^{\theta^*} \circ \Pi(X) dX \\ &= \int \nabla_{\theta}^2 q^{\theta^*} \circ \Pi(X) dX \\ &= \nabla_{\theta}^2 \int q^{\theta^*} \circ \Pi(X) dX \\ &= \nabla_{\theta}^2 1 \\ &= 0 \end{aligned}$$

□

Let F_N denote the cumulative distribution function (CDF) of $\hat{\theta}_N$ and let F denote the CDF of a normal random variable $\mathcal{N}(\mu, \sigma^2)$ with mean μ_0 and variance σ^2 . We say that

$$\hat{\theta}_N \xrightarrow{D} \mathcal{N}(\mu_0, \sigma^2)$$

if

$$\lim_{N \rightarrow \infty} F_N(t) = F(t)$$

at all t for which F is continuous.

Theorem 1.1.1. 1. Under certain conditions,

$$\sqrt{NI^{-1}(\theta^*)}(\hat{\theta}_N - \theta^*) \xrightarrow{D} \mathcal{N}(0, \mathbb{I}),$$

where

$$I(\theta^*) = (\mathcal{F}_1(\theta^*))^{-tr} \mathcal{F}_2(\theta^*) \mathcal{F}_1(\theta^*)^{-1}.$$

2. If \mathcal{F}_1 and \mathcal{F}_2 is estimated by

$$\begin{aligned} \hat{\mathcal{F}}_1(\hat{\theta}_N) &= -\frac{1}{N} \sum_{i=1}^N \nabla_{\theta}^2 \log q^{\theta} \circ \Pi(X_i) \Big|_{\theta=\hat{\theta}_N}, \\ \hat{\mathcal{F}}_2(\hat{\theta}_N) &= \frac{1}{N} \sum_{i=1}^N (\nabla_{\theta} \log q^{\theta} \circ \Pi(X_i)) (\nabla_{\theta} \log q^{\theta} \circ \Pi(X_i))^{tr} \Big|_{\theta=\hat{\theta}_N}. \end{aligned}$$

Then we have

$$\sqrt{N\hat{I}^{-1}(\hat{\theta}_N)}(\hat{\theta}_N - \theta^*) \xrightarrow{D} \mathcal{N}(\vec{0}, \mathbb{I}),$$

where

$$\hat{I}(\hat{\theta}_N) = (\hat{\mathcal{F}}_1(\hat{\theta}_N))^{-tr} \hat{\mathcal{F}}_2(\hat{\theta}_N) (\hat{\mathcal{F}}_1(\hat{\theta}_N))^{-1}.$$

Proof. Let's define a score function

$$\ell_N(\theta) = \frac{1}{N} \sum_{i=1}^N \log q^\theta \circ \Pi(X_i).$$

We notice that $\hat{\theta}_N = \arg \max_{\theta} \ell_N(\theta)$ by definition. If we assume the gradient of the score function with respect to θ exists, then the gradient of $\ell_N(\theta)$ at $\hat{\theta}_N$ must be zero.

$$\nabla_{\theta} \ell_N(\hat{\theta}_N) = \vec{0}.$$

Then use Taylor expansion to expand $\nabla_{\theta} \ell_N(\hat{\theta}_N)$ at θ^* , that is

$$\vec{0} = \nabla_{\theta} \ell_N(\hat{\theta}_N) = \nabla_{\theta} \ell_N(\theta^*) + \nabla_{\theta}^2 \ell_N(\bar{\theta})(\hat{\theta}_N - \theta^*),$$

where $\hat{\theta}_N \leq \bar{\theta} \leq \theta^*$. Assume $-\nabla_{\theta}^2 \ell_N(\bar{\theta})$ is invertible and rearrange the equation to get

$$\sqrt{N}(\hat{\theta}_N - \theta^*) = (-\nabla_{\theta}^2 \ell_N(\bar{\theta}))^{-1}(\sqrt{N}\nabla_{\theta} \ell_N(\theta^*)).$$

Let $Y_i := \nabla_{\theta} \log q^\theta \circ \Pi(X_i)|_{\theta=\theta^*}$, then $\sqrt{N}\nabla_{\theta} \ell_N(\theta^*) = \sqrt{N}\bar{Y}$. Y_i 's are i.i.d random variables with mean $\vec{0}$ by Corollary 1.1.1 and variance $\mathcal{F}_2(\theta^*)$. By the Central Limit Theorem, we have the convergence in distribution

$$\sqrt{N}\nabla_{\theta} \ell_N(\theta^*) \xrightarrow{D} \mathcal{N}(\vec{0}, \mathcal{F}_2(\theta^*)).$$

By Corollary 1.1.2, $\hat{\theta}_N \xrightarrow{P} \theta^*$ as $N \rightarrow \infty$. Because $\hat{\theta}_N \leq \bar{\theta} \leq \theta^*$, $\bar{\theta} \xrightarrow{P} \theta^*$. And by the Law of Large Number, we have the convergence $-\nabla_{\theta}^2 \ell_N(\bar{\theta}) \xrightarrow{P} \mathcal{F}_1(\bar{\theta})$. If \mathcal{F}_1 is continuous, $\mathcal{F}_1(\bar{\theta}) \xrightarrow{P} \mathcal{F}_1(\theta^*)$. Thus

$$-\nabla_{\theta}^2 \ell_N(\bar{\theta}) \xrightarrow{P} \mathcal{F}_1(\theta^*).$$

Using Slutsky's theorem to combine these two convergences together yields

$$\sqrt{N}(\hat{\theta}_N - \theta^*) \xrightarrow{D} \mathcal{N}(\vec{0}, (\mathcal{F}_1(\theta^*))^{-tr} \mathcal{F}_2(\theta^*) (\mathcal{F}_1(\theta^*))^{-1}).$$

This proves the theorem 1.1.1. \square

1.2 Asymptotic theorems for time-series data

In this section, we assume fine-scale data

$$X_0^N := (X_0, X_1, \dots, X_N),$$

being time-series data, generated by an unknown Markovian model P with time invariant transition probability $p(x, x')$ and stationary distribution $\mu(x)$. That is

$$P(X_0^N) = \mu(X_0)p(X_0, X_1)p(X_1, X_2) \dots p(X_{N-1}, X_N).$$

Here we assume X_0 starts in stationary measure.

We can get the optimal coarse grained model by minimizing the Relative Entropy Rate

$$\mathcal{H}(P|Q^\theta \circ \Pi) := \mathbb{E}_{\mu} \left[\sum_{X'} p(X, X') \log \frac{p(X, X')}{q^\theta \circ \Pi(X, X')} \right]. \quad (4)$$

In addition, the RER $\mathcal{H}(P|Q^\theta \circ \Pi)$ has an unbiased estimator $\hat{H}_N(p|q^\theta \circ \Pi)$

$$\hat{H}_N(P|Q^\theta \circ \Pi) := \frac{1}{N} \sum_{i=0}^{N-1} \log \frac{p(X_i, X_{i+1})}{q^\theta \circ \Pi(X_i, X_{i+1})}. \quad (5)$$

Thus the minimization of RER (4) is asymptotically equivalent to the optimization problem

$$\min_{\theta} \hat{H}_N(P|Q^\theta \circ \Pi) = \max_{\theta} \frac{1}{N} \sum_{i=0}^{N-1} \log q^\theta \circ \Pi(X_i, X_{i+1}).$$

Similarly define

$$\ell_N(\theta) := \frac{1}{N} \sum_{i=0}^{N-1} \log q^\theta \circ \Pi(X_i, X_{i+1}). \quad (6)$$

$$\theta^* := \arg \min_{\theta} \mathcal{H}(P|Q^\theta \circ \Pi),$$

$$\hat{\theta}_N := \arg \max_{\theta} \frac{1}{N} \sum_{i=0}^{N-1} \log q^\theta \circ \Pi(X_i, X_{i+1}).$$

Corollary 1.2.1.

$$\mathbb{E}_{\mu} \left[\sum_{X'} p(X, X') \nabla_{\theta} \log q^\theta \circ \Pi(X, X') \Big|_{\theta=\theta^*} \right] = 0.$$

Proof. It could be directly proved by taking the gradient in Eq. (4) and use the fact that θ^* is the argument of the minimum. \square

Corollary 1.2.2 (Consistency of the estimator). *Suppose that*

$$\sup_{\theta \in \Theta} |\hat{H}_N(P|Q^\theta \circ \Pi) - \mathcal{H}(P|Q^\theta \circ \Pi)| \xrightarrow{P} 0,$$

and that for every $\epsilon > 0$,

$$\sup_{\theta: |\theta - \theta^*| \geq \epsilon} \mathcal{H}(P|Q^\theta \circ \Pi) > \mathcal{H}(P|Q^{\theta^*} \circ \Pi).$$

Then we have the consistency of the estimator,

$$\hat{\theta}_N \xrightarrow{P} \theta^* \quad \text{as } N \rightarrow \infty$$

Proof. Proof is same as the proof of Corollary 1.1.2. \square

Corollary 1.2.3. *If X_i is a Markov chain with stationary distribution $\mu(x)$ and transition probability $p(x, x')$. Then*

$$S_i = (X_i, X_{i+1}) \text{ is also a Markov chain}$$

with stationary distribution

$$\mu'((x_1, x_2)) = \mu(x_1)p(x_1, x_2)$$

and transition probability

$$p'((x_1, x_2), (x'_1, x'_2)) = \begin{cases} p(x_2, x'_2) & \text{if } x_2 = x'_1 \\ 0 & \text{otherwise} \end{cases}.$$

Proof. X_i follows

$$\int \mu(X_i)p(X_i, X_{i+1})dX_i = \mu(X_{i+1}), \quad \text{for all } i.$$

Multiply the above equation by $p'((X_i, X_{i+1}), (X_{i+1}, X_{i+2}))$ to get

$$\int \mu(X_i)p(X_i, X_{i+1})p'((X_i, X_{i+1}), (X_{i+1}, X_{i+2}))dX_i = \mu(X_{i+1})p'((X_i, X_{i+1}), (X_{i+1}, X_{i+2})),$$

that is

$$\int \mu'((X_i, X_{i+1}))p'((X_i, X_{i+1}), (X_{i+1}, X_{i+2}))dX_i = \mu'((X_{i+1}, X_{i+2})) \quad \text{for all } i.$$

Clearly $S_i = (X_i, X_{i+1})$ is a Markov chain with stationary distribution μ' and transition probability p' . \square

Two Fisher information matrices are defined as

$$\mathcal{F}_1(\theta^*) := -\mathbb{E}_{\mu'}[\nabla_{\theta}^2 \log q^{\theta} \circ \Pi(X, X')|_{\theta=\theta^*}], \quad (7a)$$

$$\mathcal{F}_2(\theta^*) := \mathbb{E}_{\mu'}[(\nabla_{\theta} \log q^{\theta} \circ \Pi(X, X'))(\nabla_{\theta} \log q^{\theta} \circ \Pi(X, X'))^T|_{\theta=\theta^*}]. \quad (7b)$$

Note that here $\mathbb{E}_{\mu'}[\cdot] = \int \int \mu'(X, X')(\cdot)dXdX'$

Corollary 1.2.4. *If $p = q^{\theta^*} \circ \Pi$, then*

$$\mathcal{F}_1(\theta^*) = \mathcal{F}_2(\theta^*)$$

Proof. It is similar to the proof in Corollary 1.1.3.

$$-\nabla_{\theta}^2 \log q^{\theta} \circ \Pi(X, X') = (\nabla_{\theta} \log q^{\theta} \circ \Pi(X, X'))(\nabla_{\theta} \log q^{\theta} \circ \Pi(X, X'))^{tr} - \frac{\nabla_{\theta}^2 q^{\theta} \circ \Pi(X, X')}{q^{\theta} \circ \Pi(X, X')}.$$

Take expectation with respect to μ' at $\theta = \theta^*$ on both sides, yields

$$\mathcal{F}_1(\theta^*) = \mathcal{F}_2(\theta^*) - \mathbb{E}_{\mu'} \left[\frac{\nabla_{\theta}^2 q^{\theta} \circ \Pi(X, X')}{q^{\theta} \circ \Pi(X, X')} \Big|_{\theta=\theta^*} \right].$$

If $p = q^{\theta^*} \circ \Pi$, the last term

$$\begin{aligned} \mathbb{E}_{\mu'} \left[\frac{\nabla_{\theta}^2 q^{\theta} \circ \Pi(X, X')}{q^{\theta} \circ \Pi(X, X')} \Big|_{\theta=\theta^*} \right] &= \int \int \mu(X)p(X, X') \frac{\nabla_{\theta}^2 q^{\theta^*} \circ \Pi(X, X')}{q^{\theta^*} \circ \Pi(X, X')} dXdX' \\ &= \int \int \mu(X) \nabla_{\theta}^2 q^{\theta^*} \circ \Pi(X, X') dXdX' \\ &= \nabla_{\theta}^2 \int \int \mu(X) q^{\theta^*} \circ \Pi(X, X') dXdX' \\ &= \nabla_{\theta}^2 1 \\ &= 0 \end{aligned}$$

\square

Theorem 1.2.1. *If Markov chain (X_i) is finite or bounded and functional $\nabla_\theta(q^\theta \circ \Pi)$ has finite second moment, then*

$$\sqrt{N}(\hat{\theta}_N - \theta^*) \xrightarrow{D} \mathcal{N}(0, I(\theta^*)),$$

where

$$I(\theta^*) = (\mathcal{F}_1(\theta^*))^{-T} \Sigma(\theta^*) \mathcal{F}_1(\theta^*)^{-1},$$

$$\begin{aligned} \Sigma(\theta^*) &= E_{\mu'}[(\nabla_\theta \log q^\theta(\Pi X_0, \Pi X_1))(\nabla_\theta \log q^\theta(\Pi X_0, \Pi X_1))^T]_{|\theta=\theta^*} \\ &\quad + 2 \sum_{i=1}^{\infty} E_{\mu'}[(\nabla_\theta \log q^\theta(\Pi X_i, \Pi X_{i+1}))(\nabla_\theta \log q^\theta(\Pi X_i, \Pi X_{i+1}))^T]_{|\theta=\theta^*}, \end{aligned}$$

and $\mu'(X, X') := \mu(X)p(X, X')$.

Proof. It is similar to the proof of Theorem 1.1.1, but here we need Markov chain Central Limit theorem([26]). We still define a score function

$$\ell_N(\theta) = \frac{1}{N} \sum_{i=0}^{N-1} \log q^\theta(\Pi X_i, \Pi X_{i+1}).$$

$\hat{\theta}_N = \arg \max_\theta \ell_N(\theta)$ by definition. If we assume the gradient of the score function with respect to θ exists, then the gradient of $\ell_N(\theta)$ at $\hat{\theta}_N$ must be zero.

$$\nabla_\theta \ell_N(\hat{\theta}_N) = \vec{0}.$$

Then use Taylor expansion to expand $\nabla_\theta \ell_N(\hat{\theta}_N)$ at θ^* .

$$\vec{0} = \nabla_\theta \ell_N(\hat{\theta}_N) = \nabla_\theta \ell_N(\theta^*) + \nabla_{\bar{\theta}}^2 \ell_N(\bar{\theta})(\hat{\theta}_N - \theta^*),$$

where $\hat{\theta}_N \leq \bar{\theta} \leq \theta^*$. Assume $-\nabla_{\bar{\theta}}^2 \ell_N(\bar{\theta})$ is invertible and rearrange the equation to get

$$\sqrt{N}(\hat{\theta}_N - \theta^*) = (-\nabla_{\bar{\theta}}^2 \ell_N(\bar{\theta}))^{-1}(\sqrt{N}\nabla_\theta \ell_N(\theta^*)).$$

Now let $Y_i = \nabla_\theta \log q^\theta(\Pi X_i, \Pi X_{i+1})_{|\theta=\theta^*}$, then $\sqrt{N}\nabla_\theta \ell_N(\theta^*) = \sqrt{N}\bar{Y}$. Y_i 's are functionals of Markov chains. The conditions which guarantee the Central Limit Theorem for Y_i 's are discussed in Jones's paper [26]. In our case, if X_i is finite or bounded, then X_i is uniformly ergodic Markov chain, as well as (X_i, X_{i+1}) . If $\mathcal{F}_2(\theta^*)$ is finite, i.e., the second moment of functional of the Markov chain is finite, then we have the central limit theorem:

$$\sqrt{N}\bar{Y} \xrightarrow{D} \mathcal{N}(\vec{0}, \Sigma(\theta^*)),$$

where

$$\begin{aligned} \Sigma(\theta^*) &:= Var(Y_0) + \sum_{i=1}^{\infty} Cov(Y_0, Y_i) \\ &= E_{\mu'}[(\nabla_\theta \log q^\theta(\Pi X_0, \Pi X_1))(\nabla_\theta \log q^\theta(\Pi X_0, \Pi X_1))^{tr}]_{|\theta=\theta^*} \\ &\quad + 2 \sum_{i=1}^{\infty} E_{\mu'}[(\nabla_\theta \log q^\theta(\Pi X_i, \Pi X_{i+1}))(\nabla_\theta \log q^\theta(\Pi X_i, \Pi X_{i+1}))^{tr}]_{|\theta=\theta^*}. \end{aligned}$$

Here $\mu'(X_i, X_{i+1}) = \mu(X_i)p(X_i, X_{i+1})$. The mean is $\vec{0}$ by Corollary 1.2.1. By Corollary 1.2.2, $\hat{\theta}_N \xrightarrow{P} \theta^*$ as $N \rightarrow \infty$. Since $\hat{\theta}_N \leq \bar{\theta} \leq \theta^*$, $\bar{\theta} \xrightarrow{P} \theta^*$. And, by the Law of Large Numbers, we have the convergence $-\nabla_{\bar{\theta}}^2 \ell_N(\bar{\theta}) \xrightarrow{P} \mathcal{F}_1(\bar{\theta})$. If \mathcal{F}_1 is continuous,

$$-\nabla_{\bar{\theta}}^2 \ell_N(\bar{\theta}) \xrightarrow{P} \mathcal{F}_1(\theta^*).$$

Using Slutsky's theorem to combine these two convergences together yields

$$\sqrt{N}(\hat{\theta}_N - \theta^*) \xrightarrow{D} \mathcal{N}(\vec{0}, (\mathcal{F}_1(\theta^*))^{-T} \Sigma(\theta^*) (\mathcal{F}_1(\theta^*))^{-1}).$$

This proves the theorem 1.2.1. \square

Corollary 1.2.5. *If $\mathcal{F}_1(\theta^*)$ is estimated by*

$$\hat{\mathcal{F}}_1(\hat{\theta}_N) = -\frac{1}{N} \sum_{i=0}^{N-1} \nabla_{\hat{\theta}}^2 \log q^{\theta} \circ \Pi(X_i, X_{i+1})|_{\theta=\hat{\theta}_N},$$

and $\Sigma(\theta^*)$ is estimated by batch means([27]) assuming $N(N=ab)$ data are broken into b batch of equal size a that are assumed to be approximately independent.

$$\hat{\Sigma}_{BM} = \frac{b}{a-1} \sum_{j=1}^a (\bar{Y}_j - \bar{Y})(\bar{Y}_j - \bar{Y})^T,$$

where

$$\begin{aligned} \bar{Y}_j &= \frac{1}{b} \sum_{i=(j-1)b}^{jb-1} \nabla_{\theta} \log q^{\theta}(\Pi X_i, \Pi X_{i+1})|_{\theta=\hat{\theta}_N}, \\ \bar{Y} &= \frac{1}{N} \sum_{i=0}^{N-1} \nabla_{\theta} \log q^{\theta}(\Pi X_i, \Pi X_{i+1})|_{\theta=\hat{\theta}_N}. \end{aligned}$$

Then we have

$$\sqrt{N \hat{I}^{-1}(\hat{\theta}_N)}(\hat{\theta}_N - \theta^*) \xrightarrow{D} \mathcal{N}(0, \mathbb{I}),$$

where

$$\hat{I}(\hat{\theta}_N) = (\hat{\mathcal{F}}_1(\hat{\theta}_N))^{-T} \hat{\Sigma}_{BM}(\hat{\theta}_N) (\hat{\mathcal{F}}_1(\hat{\theta}_N))^{-1}.$$

2 Test-bed 1: Two-scale diffusion processes

2.1 Invariant and transition probability density functions

Denote $\sigma = (x, y)^{tr}$ and $\sigma_t^\epsilon := (X_t^\epsilon, Y_t^\epsilon)^T$, $a(\sigma) = \begin{pmatrix} -y \\ -\epsilon^{-1}(y-x) \end{pmatrix}$, and $b = \begin{pmatrix} 1 & 0 \\ 0 & \epsilon^{-1/2} \end{pmatrix}$. Then the two-scale diffusion SDE system is rewritten as

$$d\sigma_t^\epsilon = a(\sigma_t^\epsilon)dt + b d\mathbf{W}_t, \tag{8}$$

where $\mathbf{W}_t = (W_t^1, W_t^2)$, with W_t^1 and W_t^2 are independent standard Wiener processes. We consider an approximation $p_h(\sigma, \sigma')$ of the exact transition probability $p(\sigma, \sigma')$ of the process σ_t^ϵ , by applying

the Euler-Maruyama discretization scheme to (8). That is, for the time step $\delta t = h$, the probability to be at state σ' after time h , given that the system is at σ is

$$p_h(\sigma, \sigma') = \frac{1}{Z} e^{-\frac{1}{2}[\sigma' - \sigma - a(\sigma)h]^\top b^{-2}(\sigma' - \sigma - a(\sigma)h)}, \quad \sigma = (x, y), \quad \sigma' = (x', y'). \quad (9)$$

The invariant probability density function $\bar{\mu}^\theta(x)$ for the process X_t^{CG} satisfying equation

$$dX_t^{CG} = a(X_t^{CG}; \theta)dt + dW_t,$$

is given by the solution of the corresponding stationary Fokker-Planck equation

$$-\frac{d}{dx} \left[a(x; \theta) \bar{\mu}^\theta(x) - \frac{1}{2} \frac{d\bar{\mu}^\theta(x)}{dx} \right] = 0.$$

Under appropriate boundary conditions and the normalization $\int \bar{\mu}^\theta(x) dx = 1$, we obtain

$$\bar{\mu}^\theta(x) = \frac{1}{Z^\theta} e^{-2\bar{U}(x; \theta)}, \quad (10)$$

where $\bar{U}(x; \theta)$ is defined by $-\frac{d}{dx}\bar{U}(x; \theta) := a(x; \theta)$ and $Z^\theta = \int e^{-2\bar{U}(x; \theta)} dx$.

The transition probability of the CG process X_t^{CG} is approximated by $\bar{q}_h^\theta(x, x')$, for a discrete time step $\delta t = h$,

$$\bar{q}_h^\theta(x, x') \sim e^{-\frac{1}{2}|x' - x - a(x; \theta)h|^2}. \quad (11)$$

2.2 Relative Entropy Rate minimization reduces to Force Matching

For the two-scale diffusion process, we here show that the RER minimization, i.e., by using the transition probability, reduces to the force matching. Denote $\Delta(\sigma) = \sigma + \mathbf{a}(\sigma)h$ and recall that the CG map is the orthogonal projection $\Pi\sigma = x$. Then (9) is decomposed as

$$p_h(\sigma, \sigma') d\sigma' = \frac{1}{Z} e^{-\frac{1}{2}|\Pi\sigma' - \Pi\Delta(\sigma)|^2} dx' \times \frac{1}{\bar{Z}} e^{-\frac{\epsilon}{2}|\Pi^\perp\sigma' - \Pi^\perp\Delta(\sigma)|^2} dy',$$

where Π^\perp is the orthogonal complement of Π , i.e. $\sigma = \Pi\sigma + \Pi^\perp\sigma$ for any σ . Meanwhile, we define the (non-unique) transition probability for the CG model in the original state space

$$q_h^\theta(\sigma, \sigma') = \bar{q}_h^\theta(\Pi\sigma, \Pi\sigma') v(\sigma' | \Pi\sigma'),$$

where $\bar{q}_h^\theta(\Pi\sigma, \Pi\sigma')$ is defined in (11), and $v(\sigma' | \Pi\sigma')$ is a non-unique back-mapping probability density. Then minimizing the RER $\min_\theta \mathcal{H}(P|Q^\theta)$ is equivalent to

$$\min_\theta \left\{ - \int \int \mu(\sigma) p_h(\sigma, \sigma') \log q_h^\theta(\sigma, \sigma') d\sigma d\sigma' \right\},$$

and if we ignore the terms which are independent of θ ,

$$\min_\theta \left\{ - \int \int \mu(\sigma) p_h(\sigma, \sigma') \log \bar{q}_h^\theta(\Pi\sigma, \Pi\sigma') d\sigma d\sigma' \right\}.$$

Integrate over σ'_2 to get

$$\min_\theta \left\{ - \int \int \frac{1}{Z} e^{-|\Pi\sigma' - \Pi\Delta(\sigma)|^2} \log \bar{q}_h^\theta(\Pi\sigma', \Pi\sigma') d\sigma'_1 \mu(\sigma) d\sigma \right\}.$$

It is equivalent to

$$\min_{\theta} \int \int e^{-|\Pi\sigma' - \Pi\Delta(\sigma)|^2} |\Pi\sigma' - \Delta^{\theta}(\Pi\sigma)|^2 d\sigma'_1 \mu(\sigma) d\sigma.$$

If write $\Pi\sigma' - \Delta^{\theta}(\Pi\sigma) = \Pi\sigma' - \Pi\Delta(\sigma) + \Pi\Delta(\sigma) - \Delta^{\theta}(\Pi\sigma)$, then integrate over $d\sigma'_1 (= d\Pi\sigma')$, we have

$$\min_{\theta} \int |\Pi\Delta(\sigma) - \Delta^{\theta}(\Pi\sigma)|^2 \mu(\sigma) d\sigma.$$

Notice that $\Pi\Delta(\sigma) = X_t^{\epsilon} - Y_t^{\epsilon}h$ and $\Delta^{\theta}(\Pi\sigma) = X_t^{\epsilon} + a(X_t^{\epsilon}; \theta)h$, yields

$$\min_{\theta} \int |Y_t^{\epsilon} + a(X_t^{\epsilon}; \theta)|^2 \mu(\sigma) d\sigma.$$

2.3 RE minimization

For the case with i.i.d. data $\{(X_i, Y_i)\}_{i=1}^N$, samples from the microscopic stationary probability density $p_s(x, y)$. The CG mapping is $\Pi(X_i, Y_i) = X_i$ and the corresponding RE minimization problem is

$$\begin{aligned} \theta^{iid, re} &= \arg \max_{\theta} \mathbb{E}_{\mu} [\log \bar{\mu}^{\theta}] \\ &= \arg \max_{\theta} \left\{ -2\mathbb{E}_{\mu} [\bar{U}(\cdot; \theta)] - \log Z^{\theta} \right\}. \end{aligned}$$

We apply the Newton-Raphson optimization algorithm to calculate an estimation of $\hat{\theta}$. The k-th iteration of the Newton - Raphson algorithm is

$$\hat{\theta}_N^{(k+1)} = \hat{\theta}_N^{(k)} - \hat{H}^{-1}(\theta^{(k)}) \hat{J}(\theta^{(k)}),$$

where $\hat{J}(\theta)$ and $\hat{H}(\theta)$ are estimators of the Jacobian and Hessian matrix respectively. The Jacobian is

$$J(\theta) = -2\mathbb{E}_{\mu} [\nabla_{\theta} \bar{U}(\cdot; \theta)] + 2\mathbb{E}_{\bar{\mu}^{\theta}} [\nabla_{\theta} U(\cdot; \theta)],$$

an estimator of which is

$$\hat{J}(\theta) = -2\frac{1}{N} \sum_{i=1}^N \nabla_{\theta} \bar{U}(X_i; \theta) + 2\frac{1}{M} \sum_{j=1}^M \nabla_{\theta} \bar{U}(\bar{X}_j; \theta),$$

where $\{X_i = \Pi x_i\}_{i=1}^N$ is the CG projection of a sample set generated from the fine model, and $\{\bar{X}_j\}_{j=1}^M$ is a sample set generated from the coarse model, for the given value of θ . The Hessian matrix has elements

$$H_{ij} = 4\mathbb{E}_{\bar{\mu}^{\theta}} \left[\frac{\partial \bar{U}}{\partial \theta_i} \frac{\partial \bar{U}}{\partial \theta_j} \right] - 4\mathbb{E}_{\bar{\mu}^{\theta}} \left[\frac{\partial \bar{U}}{\partial \theta_i} \right] \mathbb{E}_{\bar{\mu}^{\theta}} \left[\frac{\partial \bar{U}}{\partial \theta_j} \right]$$

for which an estimator is

$$\hat{H}_{ij} = \frac{4}{N} \sum_{k=1}^N \frac{\partial \bar{U}}{\partial \theta_i}(X_k; \theta) \frac{\partial \bar{U}}{\partial \theta_j}(X_k; \theta) - \frac{4}{N} \sum_{k=1}^N \frac{\partial \bar{U}}{\partial \theta_i}(X_k; \theta) \frac{1}{N} \sum_{l=1}^N \frac{\partial \bar{U}}{\partial \theta_j}(X_l; \theta),$$

where

$$\frac{\partial \bar{U}}{\partial \theta_i}(x; \theta) = \frac{x^{i+1}}{i+1}, \quad i = 0, \dots, 4.$$

N	$\hat{\theta}$	Asymptotic $\hat{\sigma}^2$	Jackknife $\hat{\sigma}^2$	Bootstrap $\hat{\sigma}^2$	Asymptotic CI	Jackknife CI	Bootstrap CI
50	[0.0484]	[0.0205]	[0.0182]	[0.0172]	[-0.2321 0.3289]	[-0.2164 0.3132]	[-0.2084 0.3052]
	[-0.8575]	0.0654	0.0968	0.0982	[-1.3589 -0.3562]	[-1.4674 -0.2477]	[-1.4717 -0.2433]
	[-0.0340]	0.1765	0.2454	0.2276	[-0.8573 0.7894]	[-1.0049 0.9370]	[-0.9690 0.9010]
	[-0.0337]	0.0209	0.0514	0.1102	[-0.3172 0.2498]	[-0.4779 0.4104]	[-0.6845 0.6170]
	[-0.0627]	[0.0269]	[0.0500]	[0.0721]	[-0.3844 0.2589]	[-0.5009 0.3754]	[-0.5890 0.4635]
100	[-0.0323]	[0.0113]	[0.0083]	[0.0073]	[-0.2403 0.1757]	[-0.2105 0.1459]	[-0.1995 0.1349]
	[-1.1140]	0.0359	0.0469	0.0442	[-1.4853 -0.7427]	[-1.5387 -0.6894]	[-1.5263 -0.7017]
	0.3858	0.1000	0.1432	0.1377	[-0.2341 1.0057]	[-0.3560 1.1276]	[-0.3416 1.1132]
	0.0706	0.0156	0.0209	0.0288	[-0.1739 0.3152]	[-0.2128 0.3541]	[-0.2618 0.4031]
	[-0.2068]	[0.0184]	[0.0262]	[0.0363]	[-0.4729 0.0594]	[-0.5243 0.1107]	[-0.5804 0.1668]
200	[-0.1122]	[0.0053]	[0.0053]	[0.0054]	[-0.2545 0.0302]	[-0.2543 0.0300]	[-0.2558 0.0315]
	[-0.9702]	0.0167	0.0200	0.0197	[-1.2233 -0.7172]	[-1.2476 -0.6929]	[-1.2452 -0.6953]
	0.1548	0.0446	0.0631	0.0703	[-0.2592 0.5688]	[-0.3375 0.6472]	[-0.3648 0.6745]
	[-0.0587]	0.0060	0.0086	0.0085	[-0.2109 0.0935]	[-0.2404 0.1230]	[-0.2398 0.1224]
	[-0.1148]	[0.0074]	[0.0130]	[0.0144]	[-0.2839 0.0543]	[-0.3385 0.1090]	[-0.3500 0.1204]

Table 10: Asymptotic, jackknife and bootstrap estimates of the variance and 95% CI for the FM with i.i.d. data.

N		Asymptotic with FM	Jackknife with FM	Bootstrap with FM	asymptotic with RE	Jackknife with RE	Bootstrap with RE
50	$\hat{\theta}$	0.0484 -0.8575 -0.0340 -0.0337 -0.0627			-0.0117 -0.8720 -0.1158 -0.0321 0.0201		
	CI	[-0.2321 0.3289]	[-0.2164 0.3132]	[-0.2084 0.3052]	[-0.1465 0.1231]	[-0.9145 0.8912]	[-0.1704 0.1470]
		[-1.3589 -0.3562]	[-1.4674 -0.2477]	[-1.4717 -0.2433]	[-1.1165 -0.6275]	[-2.2984 0.5543]	[-1.0670 -0.6771]
		[-0.8573 0.7894]	[-1.0049 0.9370]	[-0.9690 0.9010]	[-0.4993 0.2677]	[-1.3890 1.1573]	[-0.3251 0.0934]
[-0.3172 0.2498]		[-0.4779 0.4104]	[-0.6845 0.6170]	[-0.1739 0.1096]	[-0.8599 0.7957]	[-0.1710 0.1068]	
	[-0.3844 0.2589]	[-0.5009 0.3754]	[-0.5890 0.4635]	[-0.0984 0.1386]	[-0.5091 0.5492]	[-0.0756 0.1157]	
200	$\hat{\theta}$	-0.1122 -0.9702 0.1548 -0.0587 -0.1148			0.0659 -0.9759 -0.0085 -0.0533 -0.0272		
	CI	[-0.2545 0.0302]	[-0.2543 0.0300]	[-0.2558 0.0315]	[-0.0740 0.2057]	[-0.6344 0.7661]	[-0.0520 0.1837]
		[-1.2233 -0.7172]	[-1.2476 -0.6929]	[-1.2452 -0.6953]	[-1.2574 -0.6945]	[-2.9675 1.0157]	[-1.1523 -0.7996]
		[-0.2592 0.5688]	[-0.3375 0.6472]	[-0.3648 0.6745]	[-0.5077 0.4906]	[-2.0745 2.0575]	[-0.2072 0.1902]
[-0.2109 0.0935]		[-0.2404 0.1230]	[-0.2398 0.1224]	[-0.1924 0.0858]	[-1.3104 1.2037]	[-0.1587 0.0521]	
	[-0.2839 0.0543]	[-0.3385 0.1090]	[-0.3500 0.1204]	[-0.1801 0.1258]	[-0.7309 0.6765]	[-0.0828 0.0285]	
500	$\hat{\theta}$	0.0236 -1.0240 0.0039 -0.0012 -0.0338			0.0247 -0.9827 0.0260 -0.0640 0.0001		
	CI	[-0.0663 0.1135]	[-0.0667 0.1139]	[-0.0703 0.1175]	[-0.1390 0.1151]	[-1.4482 1.5079]	[-0.0542 0.1139]
		[-1.1790 -0.8689]	[-1.1900 -0.8579]	[-1.1868 -0.8611]	[-1.2287 -0.7505]	[-4.2963 2.3272]	[-1.1491 -0.8200]
		[-0.2265 0.2342]	[-0.2477 0.2555]	[-0.2593 0.2670]	[-0.3005 0.3572]	[-3.7320 3.7412]	[-0.1631 0.1723]
[-0.0947 0.0922]		[-0.1099 0.1075]	[-0.1080 0.1056]	[-0.1345 0.1509]	[-2.0751 1.9495]	[-0.1682 0.0427]	
	[-0.1189 0.0513]	[-0.1350 0.0674]	[-0.1396 0.0721]	[-0.0913 0.0572]	[-1.1753 1.2034]	[-0.0465 0.0746]	

Table 11: Comparison of FM and RE with jackknife and bootstrap, with i.i.d. samples.

Estimator	N_p	N_t	$\hat{\theta}$				
FM	1	500	0.1207	-0.4328	-0.5375	-3.0699	-2.0022
RER	1	500	-1.5032	-6.0944	2.1876	20.4666	15.4355
FM	1	5,000	0.0050	-0.9485	0.0453	-0.0221	-0.0277
RER	1	5,000	-0.1530	-1.1251	0.1439	-0.0260	-0.0481
FM	1	50,000	0.0026	-0.9734	-0.0105	-0.0062	0.0038
RER	1	50,000	0.0746	-0.9805	0.0483	-0.0313	-0.0255
FM	10	500	0.0136	-0.8960	0.0839	-0.0339	-0.0485
PSRE	10	500	-0.3615	-1.3288	0.9739	-0.0195	-0.4129
FM	100	500	-0.0005	-0.9728	0.0058	-0.0081	-0.0005
PSRE	100	500	-0.1359	-0.7976	0.0756	-0.0803	0.0188
FM	100	5,000	-0.0003	-0.9777	0.0002	-0.0017	0.0003
PSRE	100	5,000	-0.0222	-0.9673	0.0798	-0.0223	-0.0171

Table 12: Point estimates for the correlated time-series data, with the different estimators for the PSRE and RER.

2.4 Additional numerical results

3 Test-bed 2: Effective force-fields and confidence in coarse-graining of linear polymer chains

3.1 Model parameters and functional forms of bonded and non-bonded interactions of the atomistic force-field

Non-Bonded Interactions			
$V_{LJ} = 4\epsilon \left[\left(\frac{\sigma}{r}\right)^{12} - \left(\frac{\sigma}{r}\right)^6 \right]$			
Atom Type	mass (g/mol)	σ (nm)	ϵ (kJ/mol)
CH3	15.0	0.375	0.8156
CH2	14.0	0.395	0.3827

Bonded Interactions		
$V_b(r) = \frac{1}{2}k(r - b)^2$		
Bond Type	b (nm)	k (kJ/mol/nm ²)
CH3-CH2	0.154	83736.0
CH2-CH2	0.154	83736.0

Angular Interactions		
$V_a(\theta) = \frac{1}{2}k(\theta - \theta_0)^2$		
Angle Type	θ_0 (degrees)	k (kJ/mol/rad ²)
CH3-CH2-CH2	112.00	482.319
CH2-CH2-CH2	112.00	482.319

Dihedral Interaction								
$V_d(\phi) = \sum_{n=0}^8 C_n \cos(\phi)^n$ (IUPAC/IUB convention)								
C_0 (kJ/mol)	C_1	C_2	C_3	C_4	C_5	C_6	C_7	C_8
8.33	-17.72	-2.52	30.06	18.53	-16.36	-37.36	14.45	23.44

3.2 CG force-field: Bonded interactions

Figures 16, 17, 18 depict the bonded interaction potentials, bond length, bond angle, and dihedral angle respectively, for the 3:1 coarse grained polyethylene model. The bonded interaction were estimated with the Iterative Inverse Boltzmann method.

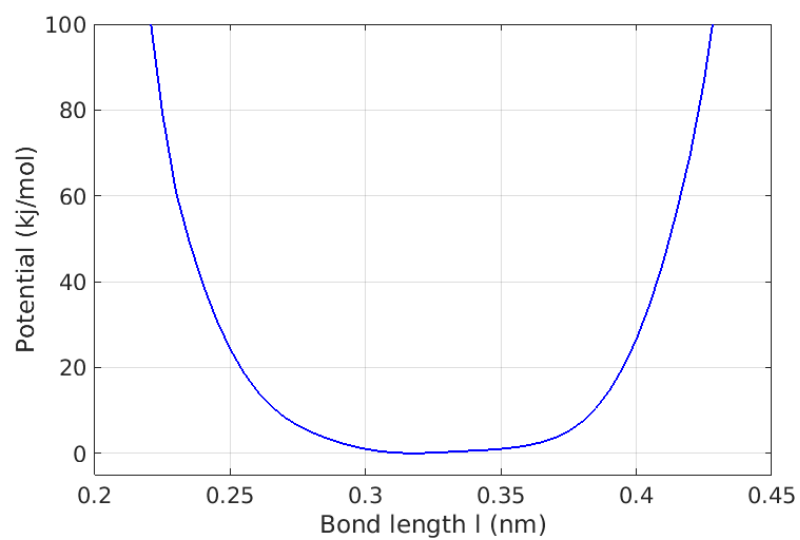


Figure 16: Bond length interaction potential

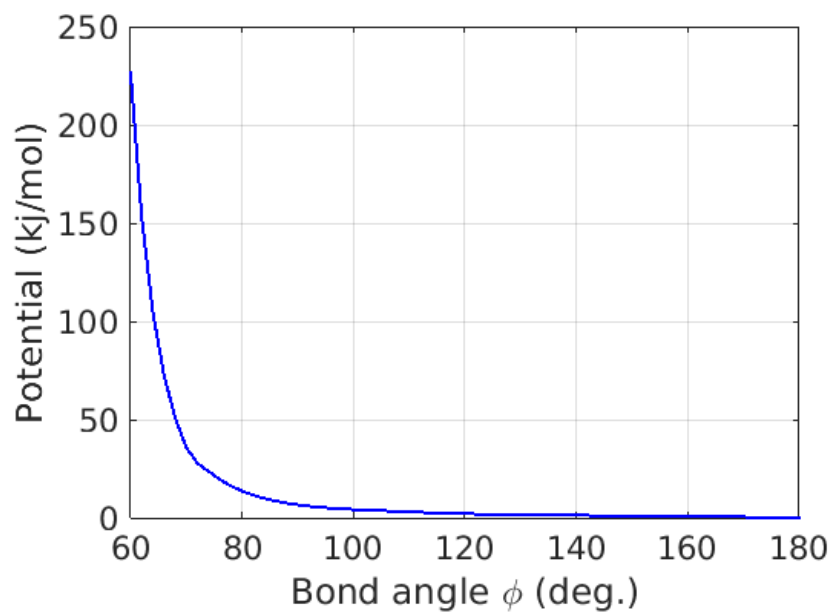


Figure 17: Bond angle interaction potential

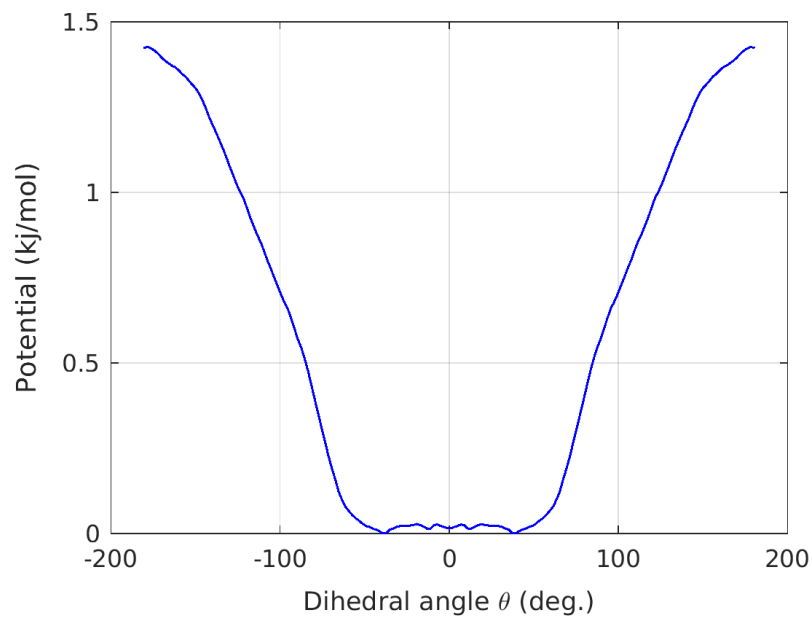


Figure 18: Dihedral angle interaction potential

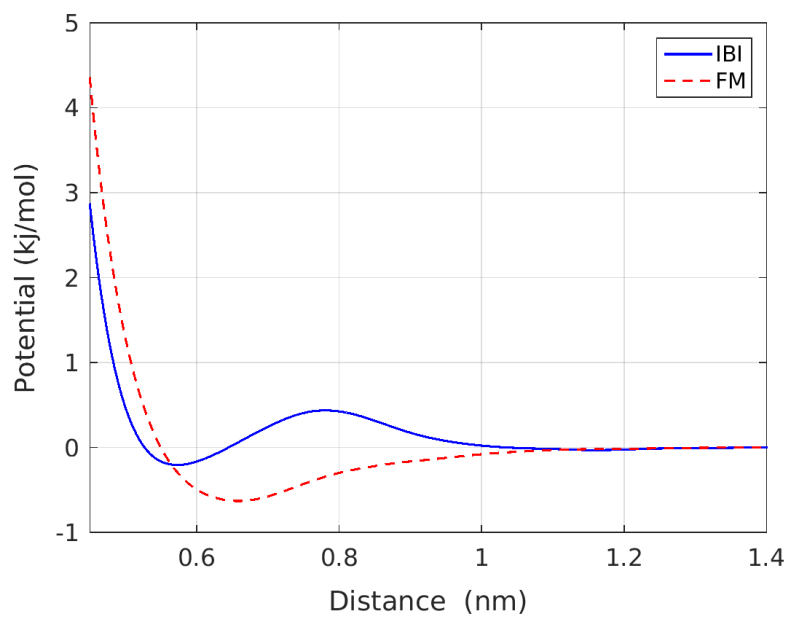


Figure 19: Comparison of the pair interaction potential $u(r)$ obtained with IBI and FM (cubic B-splines).

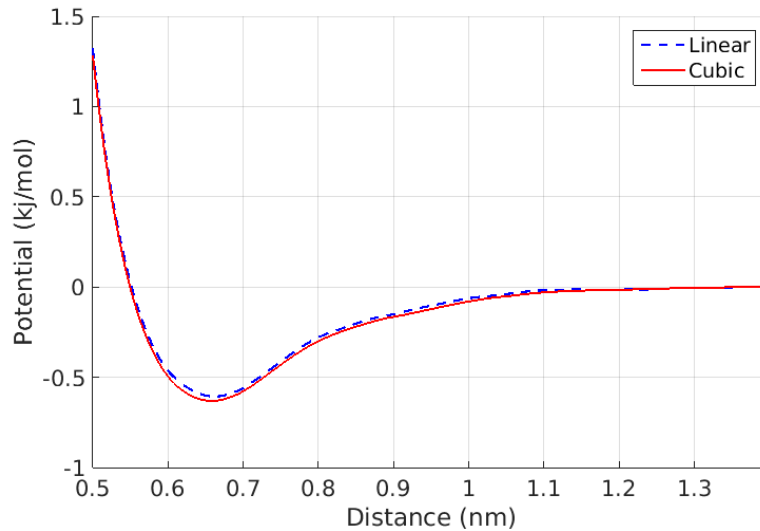


Figure 20: Pair interaction potential $u(r)$. Linear vs cubic B-splines.

3.3 CG force-field: Non-bonded interactions

Figure 20 shows a comparison of different expansions for the pair interaction potential, estimated with the FM method. The expansions we compare are linear B-splines and cubic B-splines, both with 30 parameters and both inferred from the same set of 2000 microscopic configurations. We can observe small differences between the linear and cubic splines.

Figures 21 and 22 depict the results of the FM estimation and the corresponding confidence sets for an expansion with linear B-splines and 75 parameters. We estimate the bootstrap mean and confidence intervals for a small $N_B = 300$ set of configurational samples, and $B = 300$ bootstrap samples. The parameters confidence sets are shown in the left figure of 21, depicting higher uncertainty for the first coefficients, The relative standard deviation (RSTD) for the non-zero parameters, shown in the right figure of 21.

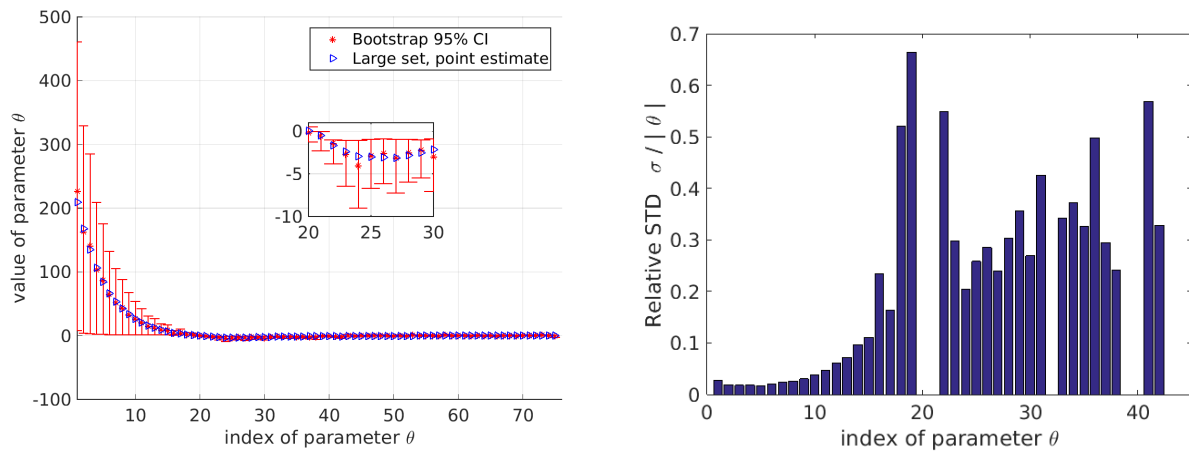


Figure 21: Linear splines, 75 parameters. Large sample (5000) vs bootstrap (300) estimates. 95% percentile CI

The 80%, 95%, and 99% bootstrap confidence intervals for the pair interaction potential are presented in figure 22, along with the point estimate of the FM method for a set of $N = 5000$ configuration samples. We present the jackknife mean and 95% confidence interval in figure 23.

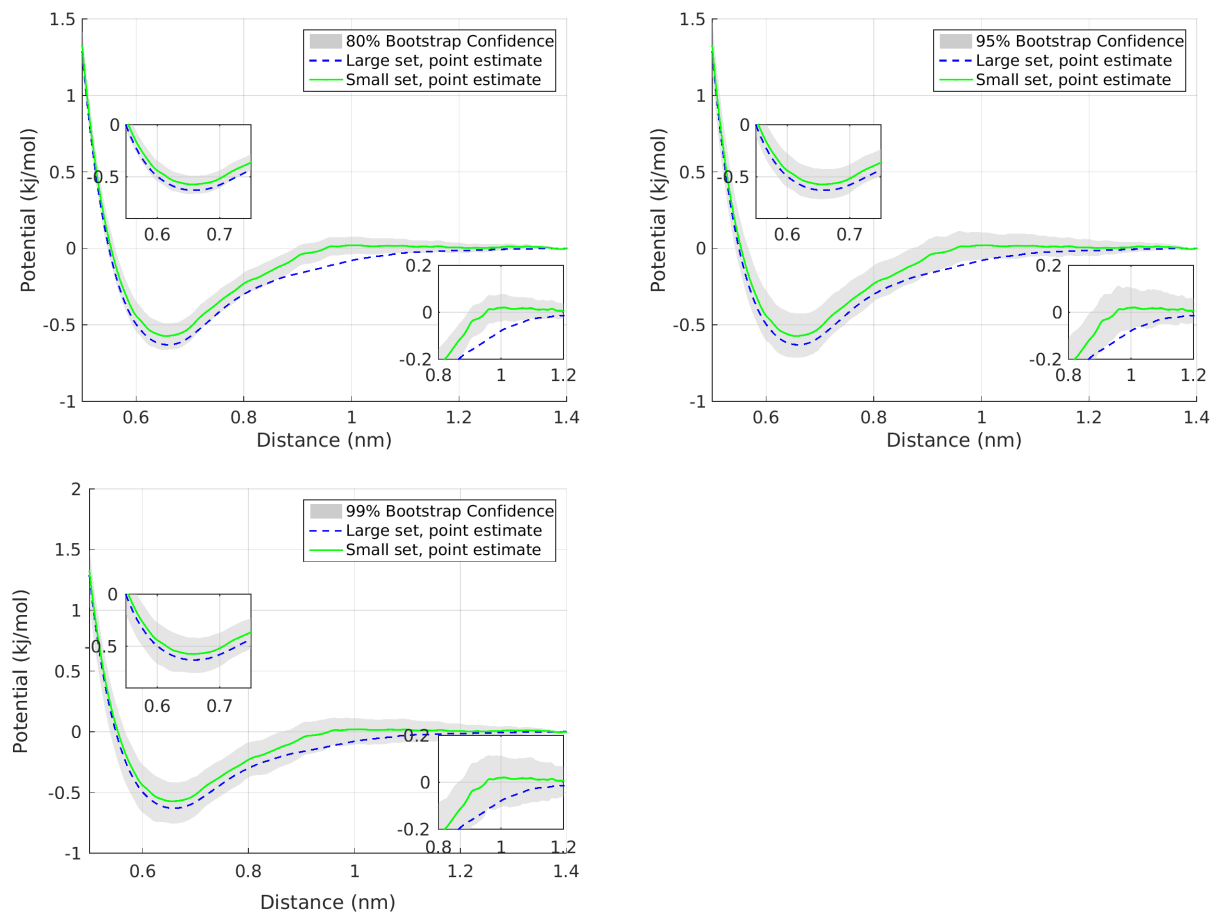


Figure 22: Pair interaction potential $u(r)$ with 80%, 95%, and 99% bootstrap confidence intervals, for linear splines with a large (5000) and a small (300) data set. The number of bootstrap samples is 300.

Figure 24 verifies that for the chosen parametric models the bootstrap and jackknife mean coincide with the point estimate. This is because the model is linear in the parameters and the model is unbiased.

References

- [1] P. Angelikopoulos, C. Papadimitriou, and P. Koumoutsakos. Bayesian uncertainty quantification and propagation in molecular dynamics simulations: A high performance computing framework. *The Journal of Chemical Physics*, 137(14):144103, 2012.
- [2] P. Angelikopoulos, C. Papadimitriou, and P. Koumoutsakos. Data driven, predictive molecular dynamics for nanoscale flow simulations under uncertainty. *The Journal of Physical Chemistry B*, 117(47):14808–14816, 2013.

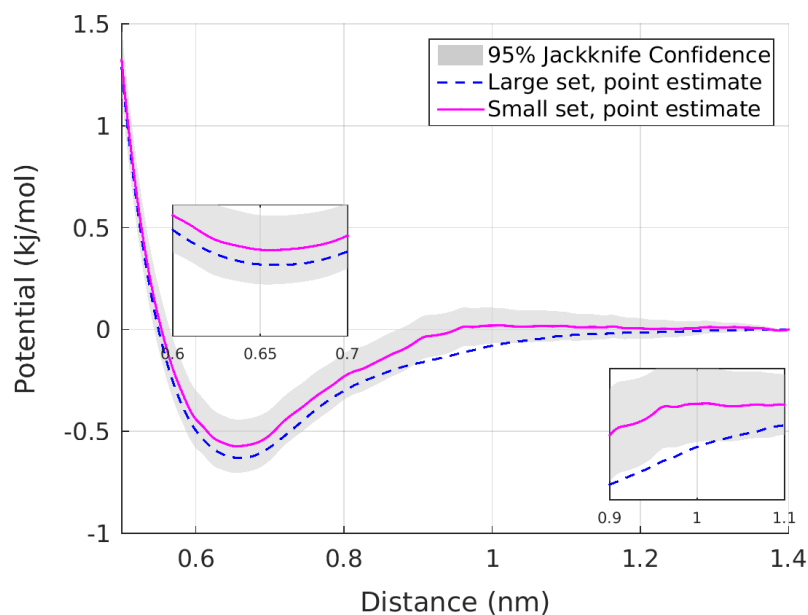


Figure 23: Pair interaction potential $u(r)$ with 95% jackknife confidence interval, for linear splines with a large (5000) and a small (300) data set.

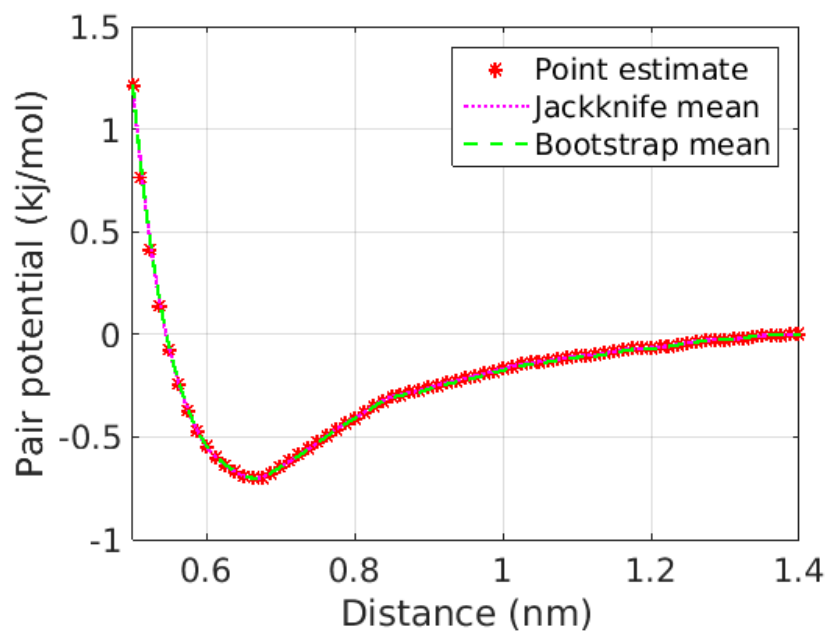


Figure 24: Pair interaction potential $u(r)$ comparison of the point estimate to the bootstrap and jackknife mean. Cubic splines with 30 parameters.

- [3] G. Casella and R.L. Berger. Statistical Inference. Duxbury advanced series in statistics and decision sciences. Thomson Learning, 2002.
- [4] A. Chaimovich and M. S. Shell. Anomalous waterlike behavior in spherically-symmetric water models optimized with the relative entropy. Phys. Chem. Chem. Phys., 11:1901–1915, 2009.
- [5] P. Bačová, E. Glynos, S. Anastasiadis, and V. Harmandaris. Nanostructuring single-molecule polymeric nanoparticles via macromolecular architecture host. ACS Nano, 13:2439–2449, 2019.
- [6] Thomas J DiCiccio and Bradley Efron. Bootstrap confidence intervals. Statistical science, pages 189–212, 1996.
- [7] M. Doi and S.F. Edwards. The Theory of Polymer Dynamics. Clarendon Press, 1986.
- [8] P. Dupuis, M. A. Katsoulakis, Y. Pantazis, and P. Plecháč. Path-space information bounds for uncertainty quantification and sensitivity analysis of stochastic dynamics. SIAM J. Uncert. Quant., 4(1):80–111, 2016.
- [9] R. Dutta, Z. F. Brotzakis, and A. Mira. Bayesian calibration of force-fields from experimental data: Tip4p water. The Journal of Chemical Physics, 149(15):154110, 2018.
- [10] B. Efron. Bootstrap methods: Another look at the jackknife. Ann. Statist., 7(1):1–26, 01 1979.
- [11] B. Efron and T. Hastie. Computer Age Statistical Inference. Institute of Mathematical Statistics Monographs. Cambridge University Press, 2016.
- [12] K. Farrell, J. T. Oden, and D. Faghihi. A Bayesian framework for adaptive selection, calibration, and validation of coarse-grained models of atomistic systems. Journal of Computational Physics, 295:189 – 208, 2015.
- [13] K. Farrell-Maupin and J. T. Oden. Adaptive selection and validation of models of complex systems in the presence of uncertainty. Research in the Mathematical Sciences, 4(1):14, Aug 2017.
- [14] L. Felsberger and P.-S. Koutsourelakis. Physics-constrained, data-driven discovery of coarse-grained dynamics. Communications in Computational Physics, 25(5):1259–1301, 2019.
- [15] S. L. Frederiksen, K. W. Jacobsen, K. S. Brown, and J. P. Sethna. Bayesian ensemble approach to error estimation of interatomic potentials. Phys. Rev. Lett., 93:165501, Oct 2004.
- [16] M.I. Freidlin, J. Szucs, and A.D. Wentzell. Random Perturbations of Dynamical Systems. Grundlehren der mathematischen Wissenschaften. Springer New York, 2012.
- [17] Jerome Friedman, Trevor Hastie, and Robert Tibshirani. The elements of statistical learning, volume 1(10). Springer series in statistics New York, 2001.
- [18] V. Harmandaris, E. Kalligiannaki, and M. Katsoulakis. Computational Design of Complex Materials Using Information Theory: From Physics- to Data-driven Multi-scale Molecular Models. ERCIM News. Special theme: Digital Twins, 115, 2018.
- [19] V. Harmandaris, E. Kalligiannaki, M. Katsoulakis, and P. Plechac. Path-space variational inference for non-equilibrium coarse-grained systems. Journal of Computational Physics, 314:355 – 383, 2016.

- [20] V. Harmandaris and K. Kremer. Dynamics of polystyrene melts through hierarchical multiscale simulations. Macromolecules, 42:791, 2009.
- [21] V. Harmandaris and K. Kremer. Predicting polymer dynamics at multiple length and time scales. Soft Matter, 5:3920, 2009.
- [22] V. Harmandaris, V. G. Mavrantzas, D. Theodorou, M. Kröger, J. Ram rez, H.C.  ttinger, and D. Vlassopoulos. Dynamic crossover from rouse to entangled polymer melt regime: Signals from long, detailed atomistic molecular dynamics simulations, supported by rheological experiments. Macromolecules, 36:1376–1387, 2003.
- [23] S Izvekov and GA Voth. Effective force field for liquid hydrogen fluoride from ab initio molecular dynamics simulation using the force-matching method. The Journal of Physical Chemistry. B, 109(14):6573–6586, 04 2005.
- [24] S. Izvekov and G.A. Voth. Multiscale coarse graining of liquid-state systems. The Journal of Chemical Physics, 123(13):134105, 2005.
- [25] L. C. Jacobson, R. M. Kirby, and V. Molinero. How Short Is Too Short for the Interactions of a Water Potential? Exploring the Parameter Space of a Coarse-Grained Water Model Using Uncertainty Quantification. The Journal of Physical Chemistry B, 118(28):8190–8202, 2014.
- [26] G. L. Jones. On the Markov chain central limit theorem. Probability surveys, 1(299-320):5–1, 2004.
- [27] G. L Jones, M. Haran, B. S Caffo, and R. Neath. Fixed-width output analysis for Markov chain Monte Carlo. Journal of the American Statistical Association, 101(476):1537–1547, 2006.
- [28] M. A. Katsoulakis and P. Plechac. Information-theoretic tools for parametrized coarse-graining of non-equilibrium extended systems. J. Chem. Phys., 139:4852–4863, 2013.
- [29] M. A. Katsoulakis and P. Vilanova. Data-driven, variational model reduction of high-dimensional reaction networks. Journal of Computational Physics, 401:108997, 2020.
- [30] Pu L., Qiang S., Hal D., and Gregory A. Voth. A Bayesian statistics approach to multiscale coarse graining. The Journal of Chemical Physics, 129(21):214114, 2008.
- [31] S. Longbottom and P. Brommer. Uncertainty quantification for classical effective potentials: an extension to potfit. Modelling and Simulation in Materials Science and Engineering, 27(4):044001, 2019.
- [32] A.P. Lyubartsev and A. Laaksonen. Calculation of effective interaction potentials from radial distribution functions: A reverse Monte Carlo approach. Phys. Rev. E, 52:3730–3737, 1995.
- [33] A.P. Lyubartsev, A. Mirzoev, L. Chen, and A. Laaksonen. Systematic coarse-graining of molecular models by the newton inversion method. Faraday Discussion, 144(1):43–56, 2010.
- [34] R. G. Miller. The Jackknife—A Review. Biometrika, 61(1):1–15, 1974.
- [35] F. M ller-Plathe. Coarse-graining in polymer simulation: From the atomistic to the mesoscopic scale and back. ChemPhysChem, 3(9):754–769, 2002.
- [36] W. G. Noid. Systematic methods for structurally consistent coarse-grained models. Methods Mol. Biol., 924(9):487–531, 2013.

- [37] W. G. Noid, J. Chu, G.S. Ayton, V. Krishna, S. Izvekov, G.A. Voth, A. Das, and H.C. Andersen. The multiscale coarse-graining method. I. A rigorous bridge between atomistic and coarse-grained models. The Journal of Chemical Physics, 128(24):244114, 2008.
- [38] W. G. Noid, Jih-Wei Chu, Gary S. Ayton, and Gregory A. Voth. Multiscale coarse-graining and structural correlations: Connections to liquid-state theory. The Journal of Physical Chemistry B, 111(16):4116–4127, 2007.
- [39] W. G. Noid, P. Liu, Y. Wang, J. Chu, G.S. Ayton S. Izvekov, H.C. Andersen, and G.A. Voth. The multiscale coarse-graining method. II. Numerical implementation for coarse-grained molecular models. The Journal of Chemical Physics, 128(24):244115, 2008.
- [40] B. Oksendal. Stochastic Differential Equations: An Introduction with Applications. Hochschultext / Universitext. U.S. Government Printing Office, 2003.
- [41] W.H. Press, S.A. Teukolsky, W.T. Vetterling, and B.P. Flannery. Numerical Recipes. Cambridge University Press, 2007.
- [42] J. Proppe and M. Reiher. Reliable estimation of prediction uncertainty for physicochemical property models. Journal of Chemical Theory and Computation, 13(7):3297–3317, 2017. PMID: 28581746.
- [43] D. Reith, M. Pütz, and F. Müller-Plathe. Deriving effective mesoscale potentials from atomistic simulations. Journal of Computational Chemistry, 24(13):1624–1636, 2003.
- [44] A. Rissanou, P. Bačová, and V. Harmandaris. Investigation of the properties of nanographene in polymer nanocomposites through molecular simulations: Dynamics and anisotropic brownian motion. PCCP, 21:23843–23854, 2019.
- [45] J. F. Rudzinski. Recent progress towards chemically-specific coarse-grained simulation models with consistent dynamical properties. Computation, 7(3), 2019.
- [46] M. Schöberl, N. Zabaras, and P.-S. Koutsourelakis. Predictive coarse-graining. Journal of Computational Physics, 333:49 – 77, 2017.
- [47] Jun Shao and CF Jeff Wu. A general theory for jackknife variance estimation. The Annals of Statistics, pages 1176–1197, 1989.
- [48] M.S. Shell. The relative entropy is fundamental to multiscale and inverse thermodynamic problems. The Journal of Chemical Physics, 129(14):–, 2008.
- [49] W. Tschöp, K. Kremer, O. Hahn, J. Batoulis, and T. Bürger. Simulation of polymer melts. I. coarse-graining procedure for polycarbonates. Acta Polym., 49:61, 1998.
- [50] A. Tsourtis, V. Harmandaris, and D. Tsagkarogiannis. Parameterization of coarse-grained molecular interactions through potential of mean force calculations and cluster expansions techniques. Entropy, 19:395, 2017.
- [51] A. Tsourtis, Y. Pantazis, M. Katsoulakis, and V. Harmandaris. Parametric sensitivity analysis for stochastic molecular systems using information theoretic metrics. The Journal of Chemical Physics, 143:014116, 2015.
- [52] L. Wasserman. All of nonparametric statistics. Springer Science & Business Media, 2006.

- [53] L. Wasserman. All of Statistics: A Concise Course in Statistical Inference. Springer Texts in Statistics. Springer New York, 2010.
- [54] T. Weymuth, J. Proppe, and M. Reiher. Statistical analysis of semiclassical dispersion corrections. Journal of Chemical Theory and Computation, 14(5):2480–2494, 2018.